14 Magnetic Resonance Imaging of the Ultrastructural Composition of Articular Cartilage in Disease and Repair

Siegfried Trattnig, Götz H. Welsch, Sebastian Röhrich, Markus M. Schreiner, and Martin Zalaudek

14.1 Introduction

Articular cartilage injuries are commonly seen in orthopedic practice. In a retrospective review of 31,510 knee arthroscopies, the incidence of chondral lesions was 63%. Full-thickness articular cartilage lesions with exposed subchondral bone were found in 20% of patients, with 5% of all arthroscopy in patients less than 40 years of age with grade IV chondral lesions [1].

The treatment of articular cartilage damage after traumatic insult or due to degenerative joint disease remains a challenge because of the limited capacity of adult cartilage for spontaneous repair [2]. Knee cartilage defects that exceed a critical size heal poorly and usually lead to osteoarthritis (OA). Several surgical and nonsurgical strategies have been developed in an attempt to repair articular cartilage lesions. The surgical techniques may be arthroscopic or open and include marrow stimulation techniques, such as drilling and microfracturing, osteochondral (OC) grafts, and cell-based techniques [3]. Refer to Chaps. 7, 11, 12, and 17 for in-depth information pertaining to the arthroscopic and surgical techniques for cartilage repair.

The high prevalence of knee cartilage lesions and disease created a strong demand for a noninvasive diagnostic tool that is reliable and reproducible. Likewise, with the variety of treatment

S. Trattnig, MD (✉)
High Field MR Center, Department of Biomedical Imaging and Image-Guided Therapy, Medical University of Vienna, Vienna, Austria

Austrian Cluster for Tissue Regeneration, Vienna, Austria

Christian Doppler Laboratory for Clinical Molecular MR Imaging, Vienna, Austria
e-mail: siegfried.trattnig@meduniwien.ac.at

G. H. Welsch, MD
Department of Athletics and Sports Medicine, University Medical Center Hamburg-Eppendorf, Hamburg, Germany

UKE Athleticum, Division of Orthopaedic Sports Medicine, University Hospital of Hamburg-Eppendorf, Hamburg, Germany

S. Röhrich, MD
High Field MR Centre, Department of Biomedical Imaging and Image-Guided Therapy, Computational Imaging Research Laboratory, Medical University of Vienna, Vienna, Austria

M. M. Schreiner, MD · M. Zalaudek, MD
Department of Orthopaedics and Trauma Surgery, Medical University of Vienna, Vienna, Austria

High Field MR Center, Department of Biomedical Imaging and Image-Guided Therapy, Medical University of Vienna, Vienna, Austria

H. K. Gahunia et al. (eds.), *Articular Cartilage of the Knee*,
https://doi.org/10.1007/978-1-4939-7587-7_14

options available to address the chondral and osteochondral lesions, there is a need for an imaging modality that offers the most sensitive and safe, noninvasive way to monitor and assess repair tissue and its integration to native cartilage following regenerative cartilage treatment. Magnetic resonance imaging (MRI) has advanced tremendously over the last several years and has offered the opportunity to fulfill this demand. Cartilage-sensitive sequences, high-resolution three-dimensional (3D) isotropic sequences, semiquantitative MR-based scores, and volumetric assessments provide invaluable information. Morphologic sequences allow diagnostic cartilage imaging with increased precision; and, in combination with volumetry and semiquantitative scores, it also allows the reproducible and repetitive MR assessment of repair tissue. However, morphological MRI is limited to the cartilage structure and does not provide any information about cartilage molecular composition. The recent development of biochemical MR imaging has filled this void by providing information about the ultrastructural elements of cartilage, such as water, collagen, and proteoglycans. In the following pages, we outline the basic principles of morphological and biochemical MRI and the current state-of-the-art clinical practice for applying these techniques to the articular cartilage of the knee.

14.2 Morphological Magnetic Resonance Imaging of Articular Cartilage

Postsurgical follow-up protocols vary and involve assessment of clinical symptoms, direct visualization of grafts with arthroscopy, or indirect visualization of grafts with MRI. For long-term follow-up of these procedures, clinical scores and the morphological and biochemical evaluation of biopsies taken during control arthroscopies remain the standard of reference [4–6]. However, considering the invasive character of arthroscopic procedures and the risk for associated morbidity, objective noninvasive measures of the properties of the grafted regions after biological cartilage repair is highly desirable and very helpful to facilitate the evaluation of longitudinal repair tissue follow-up. The purpose of cartilage imaging is to visualize the integrity of cartilage surface and its matrix; to evaluate cartilage thickness, volume, and – once cartilage repair is performed – the integration of the repair tissue to surrounding native cartilage and underlying bone. Providing these informations, morphological MRI is playing an important role in pre- and postoperative imaging as well as follow-up assessment of repair tissue throughout the postoperative period. Hence, MRI is the current standard imaging method for the noninvasive assessment of articular cartilage [5, 7–15].

In a clinical setting, the evolution of MRI technology has provided excellent contrast between articular cartilage and adjacent structures within reasonable imaging times. MR evaluation of cartilage repair can be performed using the same acquisition techniques as those used for native cartilage. In 2000, the Articular Cartilage Imaging Group (ACIG) of the International Cartilage Repair Society (ICRS) compiled an MR acquisition protocol for cartilage imaging, which has not been updated since. The most commonly used MR imaging techniques on 1.5 tesla (T), 3.0 T, and research 7 T scanners are fluid-sensitive sequences, such as two-dimensional (2D) fat-suppressed (fs), intermediate and T2-weighted (T2W) fast spin echo (FSE), as well as 3D gradient-recalled echo (GRE) techniques with fat suppression or water excitation, all in combination with dedicated extremity coils [9, 11–15, 16–18]. A minimal in-plane resolution of 0.3 mm was found to be necessary to show early signs of superficial fraying of the articular cartilage surface, which was also substantial for the detection of cartilage fissures and insufficient repair-tissue integration to native cartilage [19]. Compared to 2D, the 3D acquisition is advantageous with regard to higher contrast- and signal-to-noise ratios which also yields higher and isotropic resolutions for multi-planar reconstructions that enables 3D visualizations and volume measurements [10, 11, 16, 20].

14.2.1 Cartilage-Specific MR Sequences

Magnetic resonance imaging is the most important modality for the detection and evaluation of traumatic or degenerative cartilaginous lesions in the knee as well as for monitoring the effects of pharmacological and surgical therapy. To date, several cartilage-specific MR imaging techniques have been developed to assess the morphological integrity of knee cartilage such as FSE, 3D spin echo, and gradient echo as well as isotropic imaging.

14.2.1.1 Fast Spin Echo Technique

Fast spin echo imaging combines strong T2 weighting, magnetization transfer effects, and relative preservation of high signal intensity in the marrow fat and free water (Fig. 14.1). With FSE technique, articular cartilage is visualized as low signal intensity (dark) hence producing high contrast between cartilage and the adjacent synovial fluid and bone marrow [21, 22]. Intermediate-weighted FSE sequences are useful for both the detection of cartilage surface lesions and intrachondral extracellular matrix lesions. The FSE technique is relatively insensitive to magnetic susceptibility artifacts, which is advantageous in patients who have undergone previous surgery of the joint. FSE sequences are normally included in the clinical standard MR imaging protocol for the knee, as high-resolution images can be acquired in a relatively short scan time [12, 13, 23]. Apart from the usual 2D FSE imaging, a 3D FSE sequence has also been developed and is available if subsequent reconstructions or semiquantitative assessments are desired [24].

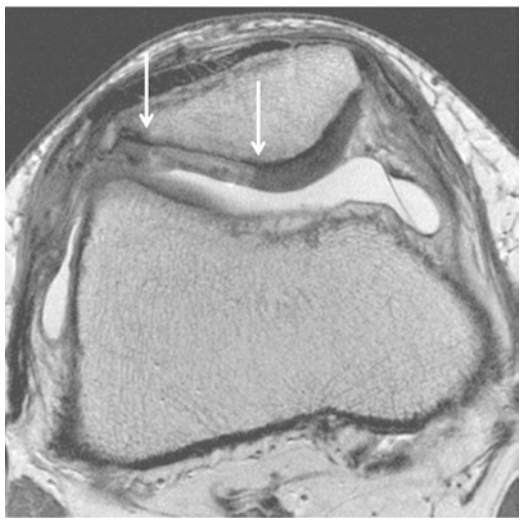

Fig. 14.1 Conventional axial proton-density-weighted (PDW) high-resolution turbo-spin-echo (TSE) MRI of a 30-year-old female patient at early follow-up of 3 months after matrix-associated chondrocyte transplantation. The arrows show inhomogeneous MR signal intensity of the repair tissue matrix. (Acquisition parameters: TR: 2400 ms; TE: 28 ms; flip angle: 160°; in-plane resolution: 0.23 × 0.23 mm; matrix: 512 × 512; slice thickness: 2 mm; slices: 34; TA: 6:01 min)

14.2.1.2 Three-Dimensional Gradient Echo Technique

Three-dimensional spoiled GRE imaging with fs or water excitation is widely available and easy to perform. This technique yield images with higher resolution and contrast-to-noise ratio (CNR) than 2D acquisitions. Contrary to other cartilage imaging techniques, 3D-GRE does not require data post-processing and avoids misregistration artifacts [9, 11, 13, 14, 16]. It exhibits a relatively high signal intensity (bright) articular cartilage in contrast to low signal intensity (dark) adjacent fat-suppressed tissue. The 3D dataset can subsequently be reformatted in any other plane for further 3D visualization and volume measurements [10, 11, 16]. However, GRE sequences are especially prone to susceptibility artifacts caused by metal abrasion which may hamper accurate cartilage evaluation in patients who have undergone arthroscopy.

14.2.1.3 Isotropic Imaging

Isotropic imaging requires 3D acquisitions of voxels with uniform length in any dimension. This isotropic dataset allows the sequence to be performed in one plane, for example, in the sagittal plane; and subsequently, it can be reformatted in all other planes, even oblique planes, without any loss of resolution. Many isotropic 3D gradient echo sequences, such as dual echo steady state (DESS), true fast imaging with steady-state precession (True-FISP), fast low angle shot (FLASH), balanced fast field echo (Balanced

FFE), volumetric interpolated breath-hold examination (VIBE), and multiple echo data image combination (MEDIC), have been developed. A voxel size down to 0.5 cm for 1.5 T with a high gradient strength has great potential for cartilage imaging.

The 3D DESS sequence has proved to be valuable for first-stage cartilage assessment [25–27]. This sequence provides an intermediate cartilage signal intensity, high cartilage-to-fluid contrast, and is suitable for quantitative volumetric measurements [28, 29]. The 3D-True-FISP sequence provides substantially higher signal-to-noise ratio (SNR) and contrast-to-noise ratio (CNR) than the 3D-FLASH sequence [30]. This advantage in signal intensity allows for higher spatial resolution and, thus, potential improvement in the accuracy of the segmentation process, especially at the articular surface [30]. With high-field MRI, this advantage might also be used to perform isotropic MR measurements in a minimal amount of time (Fig. 14.2). With the use of a dedicated, eight-channel knee coil, an isotropic (0.6 mm^3), 3D-True-FISP dataset can be assessed in approximately 3 min. The potential of 3D-True-FISP to diagnose cartilage defects and other knee soft tissue aberrations (such as anterior cruciate ligament (ACL) abnormalities and meniscal tears) can be expected to be higher than with a set of standard 2D sequences [31].

Another exciting 3D FSE sequence development is the "3D sampling perfection with application of optimized contrasts using different flip angle evolution" sequence (3D SPACE), which features isotropic voxels and consecutive reformatting in any plane without loss of resolution, and the advantages of the FSE approach (Fig. 14.3). Steady-state free precession (SSFP)-based techniques have increased SNR and CNR efficiency at 3 T MRI [32]. The True-FISP sequence, an SSFP-based sequence, was studied in detail at 1.5 T and is clinically available for morphological evaluation of cartilage [31, 33]. Compared to a 3D-FLASH and a 3D-DESS sequence, the preoperative detection of cartilage defects is possible with similar sensitivity, specificity, and accuracy for the water-excitation True-FISP sequence; however, the SSFP-based sequences show the highest SNR and CNR efficiency.

14.2.2 Quantitative Morphological Magnetic Resonance Imaging

Quantitative morphological cartilage parameters (e.g., cartilage thickness) provide more specific information and are less observer-dependent when compared to a qualitative approach. Given sufficient refinement, they may act as markers for the prediction of disease onset, progression of cartilage degeneration, or monitoring of therapeutic interventions. Quantitative morphological parameters encompass, for example, the volume of cartilage, the total area of subchondral bone,

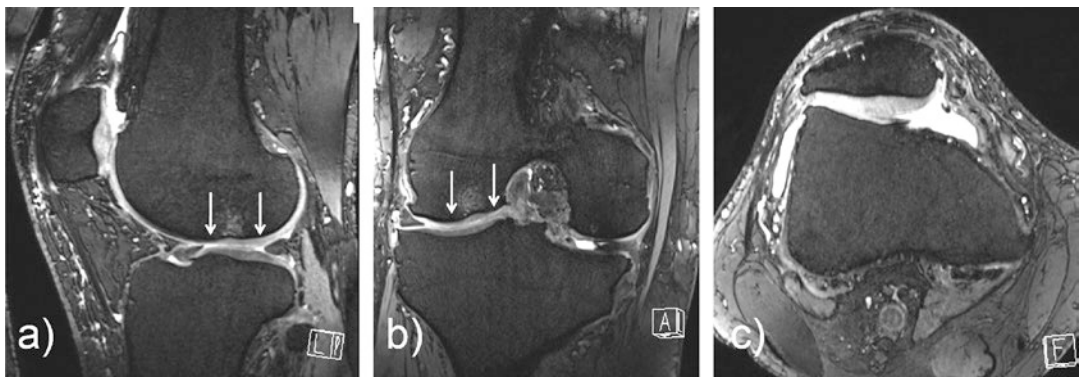

Fig. 14.2 MR images of the lateral femoral condyle of a 48-year-old male patient obtained with a 3D True FISP sequence 24 months after matrix-associated chondrocyte transplantation. Image acquisition was performed in the sagittal plane (**a**) and reconstructed in the coronal (**b**) as well as in the transversal (**c**) plane. (Acquisition parameters: TR: 8.9 ms; TE: 3.8 ms; in-plane-resolution: 0.4 × 0.4 mm; slice thickness: 0.4 mm; slices: 320; TA: 6:46 min)

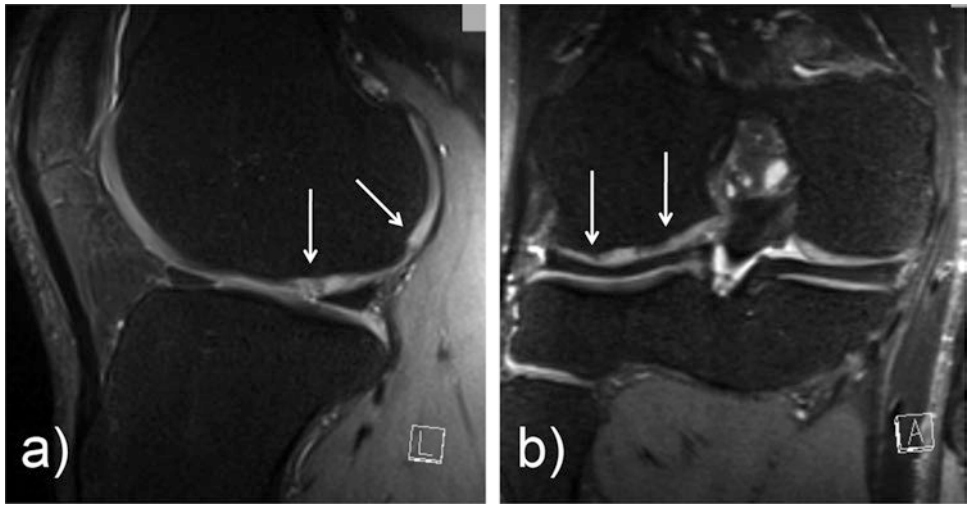

Fig. 14.3 Sagittal (**a**) and coronal (**b**) MR images acquired with a 3D-SPACE of the femoral condyle of a patient were obtained 36 months after microfracture therapy. Inhomogeneous cartilage repair tissue can be appreciated (arrows). (Acquisition parameters: TR: 1500 ms; TE: 34 ms; Resolution: 0.5 × 0.5 × 0.5 mm; slices: 192; TA: 7:53 min)

and the denuded part thereof, ratios between the aforementioned measures, and many others [34]. Clinical utility of MR pulse sequences for accurate and precise quantitative analysis of cartilage morphology in cross-sectional and longitudinal studies involving healthy subjects and OA patients has been reported [35]. Using quantitative MRI technique, the investigators examined the 4-year trajectory of femoro-tibial cartilage thickness loss (measured annually, longitudinal data) in OA patients prior to knee replacement and compared the data with that of matched controls by age, sex, and baseline radiographic stage. Accelerated cartilage loss, in particular the 2 years prior to knee replacement in OA patients compared to control subjects, was reported [35]. Other authors have investigated the possibility of quantifying bone marrow lesion volume, as well as denuded bone area, and have shown an association with the Boston Leeds Osteoarthritis Knee Score (BLOKS) [36, 37]. In a phase III clinical trial, cartilage volume loss and bone marrow lesions were used to demonstrate a beneficial effect of strontium ranelate on structural alterations in patients with symptomatic OA [38].

However, to achieve a qualified and validated imaging biomarker, many preconditions need to be fulfilled as follows:

First, the standardization in image acquisition must be ascertained. Different vendors of scanners, MR pulse sequences, and patient-specific factors contribute to a large variance in data, making it difficult to evaluate small changes in quantitative parameters. As an example, one study found that in a healthy population with a mean knee cartilage thickness of 3.8 mm, a change of 1 mm already puts an individual two standard deviations away from the mean indicating the necessity of accurate procedures to avoid losing a relevant change in the abovementioned variance [39]. A prominent project that provides a large body of standardized longitudinal data is the Osteoarthritis Initiative [40].

Second, the region or volume of interest needs to be defined. Semiquantitative scores, such as the Whole-organ Magnetic Resonance Imaging Score (WORMS) [41], suggest that knee compartments and subregions are relevant features to be evaluated. This is important, as different regions in the knee joint vary in morphological appearance [39], as well as exhibit different functional behavior [42] and dynamics in disease [43].

Third, the chosen volume of interest must be segmented. An accurate, automated approach would be preferable; however, the current consensus is that, although time-consuming, expert

segmentation with the aid of segmentation assistance is superior to the purely computational variant [44].

Finally, the further development of quantitative MR imaging biomarkers can be described by three distinctive steps [45]. *Analytical validation* leads to the demonstration of the feasible, accurate, and precise measurement of a biomarker. *Qualification* of a biomarker means the demonstration of an association with a clinical outcome. *Utilization* involves an evaluation of the practicability in clinical routine. This includes its efficient (i.e., automatic) extraction, integration into existent radiology information systems, usefulness in decision-making, and cost-effectiveness.

14.2.3 High-Resolution Magnetic Resonance Imaging

Several studies on articular cartilage have tried to optimize MR pulse sequences for the assessment of articular cartilage by selecting imaging parameters that accentuate the CNR for cartilage. However, these studies did not focus on optimizing the image resolution. Fat-suppressed, 3D GRE imaging provides a high CNR between cartilage and surrounding tissue, and 3D acquisition produces smaller voxels by decreasing the slice thickness. Still, in all sequences, a trade-off has to be made between signal-to-noise ratio, voxel size, and acquisition time. By accepting longer scan times, an in-plane resolution of 0.27– 0.31 mm could be achieved at 3 T [42]. However, the image resolution of standard MR sequences reported in the literature is inadequate to reveal fraying of the articular cartilage surface or to discriminate the smooth surface of healthy cartilage from early superficial changes in degenerative cartilage [9, 11, 13, 14, 46, 47]. Thus, an increase in in-plane resolution is necessary to reliably depict changes in the integrity of the superficial zone of articular cartilage, which is critical in the assessment of early stage of cartilage degeneration in OA. In particular, the optimal definition of the morphology of cartilage repair following matrix-based autologous cartilage implantation (ACI) benefits from high-resolution MRI (Fig. 14.4). Indeed, the thin zonal layering of cartilage necessitates high-resolution MRI and, therefore, also the implementation of specialized technical equipment.

Previously, a 1.0 or 1.5 T MR scanner with a high-performance gradient system and a dedicated extremity coil (quadrature/phased array coil) were the minimum requirements. Then, the availability of 3 T clinical MR systems for routine examinations enabled high signal-to-noise ratios and high-resolution imaging, which was subsequently surpassed by 7 T scanners [48]. In 2003, the US Food and Drug Administration (FDA) approved field strengths lower than 8 T in adults as a "nonsignificant risk" [49], facilitating the use of 7 T scanners for certain routine clinical imaging indications, and thus, the next important step in achieving even higher resolutions in MRI (Fig. 14.5a, b). For the newest generation of 7 T scanners, an isotropic spatial resolution of 0.2 mm is expected. Analogous to the advancement from 1.5 T to 3 T, qualitative and quantitative cartilage imaging will continue to be the most important aspect of 7 T MR in musculoskeletal imaging. This statement is supported by a recent study which compared the diagnostic confidence of readers between 3 T and 7 T MRI of patellar cartilage and found a significant improvement in diagnostic confidence for low-grade cartilage lesions at 7 T [50].

The MRI SNR can be partially improved by the use of dedicated extremity coils with the optimal pulse sequence to increase resolution within a given imaging time [51]. In most cases, these coils act as receive coils that offer a high SNR, which allows the application of a small field of view (FOV) and a large matrix size, resulting in an increased in-plane resolution that can be achieved within a clinically acceptable scan time.

14.2.4 Magnetic Resonance Morphologic Imaging of Repair Tissue

Since the past two decades, there has been a significant progress in the field of cartilage repair procedures. Innovative surgical techniques are

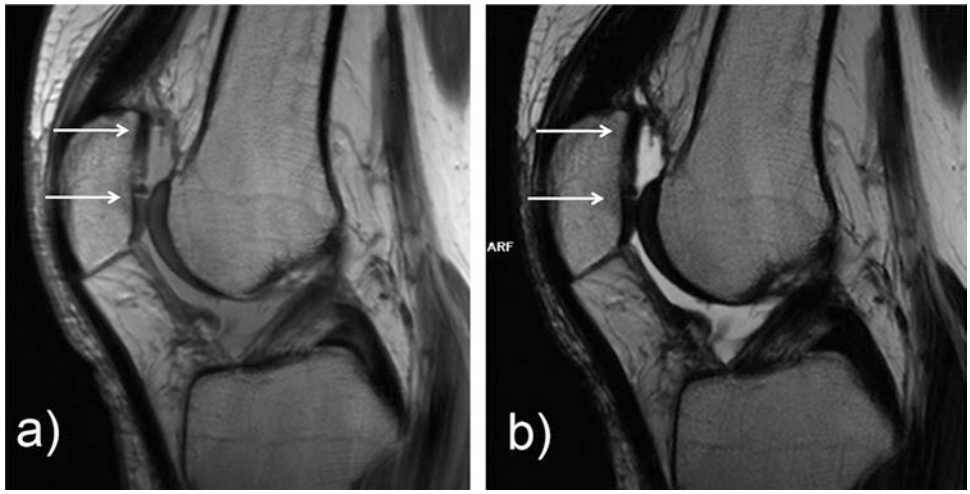

Fig. 14.4 Conventional high-resolution sagittal T2-weighted dual FSE MRI of the patello-femoral joint of a 30-year-old female patient (same patient as in Fig. 14.1) in an early follow-up three months after matrix-associated chondrocyte transplantation. (Acquisition parameters: TR: 5120 ms; TE: 9.5 ms (image **a**) and 124 ms (image **b**); flip angle: 160°; matrix size: 448 × 448; FOV: 18cm; slice thickness: 3mm; slices: 32; TA: 6:35 min). The depicted hyperintense or inhomogeneous cartilage repair tissue, and even the questionable split-like lesions of the repair tissue surface (arrows, **a**) usually disappear after 6–12 months (**b**)

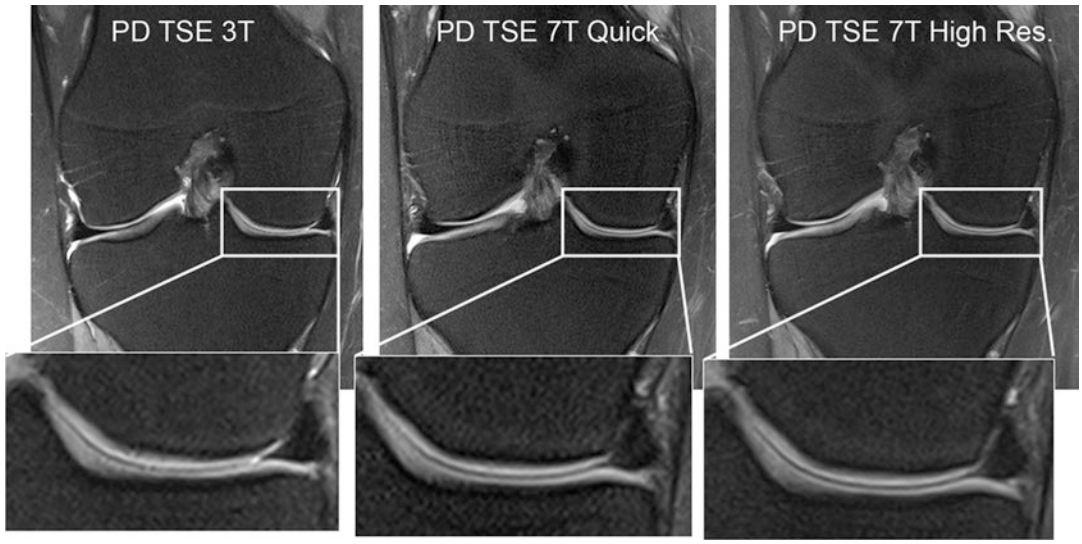

Fig. 14.5 Comparison of 3 T (left) and 7 T (middle and right) coronal MR images of the knee of a healthy volunteer acquired with a fat-saturated (fs) 2D proton-density turbo-spin-echo (PD TSE) sequence. The magnified picture detail of the medial knee compartment allows for better visualization of the image quality of the articular cartilage. The gain in SNR at 7T can be invested in faster acquisition (middle) or higher resolution at similar acquisition time (right). (Image obtained with permission from the Ref. [51])

currently available to treat patients with symptomatic, focal cartilage defect due to injury or disease. These surgical techniques include microfracture, OC auto- or allografting, matrix-induced autologous chondrocyte implantation (MACI), juvenile cartilage cell implantation, and non-cell-seeded biocompatible matrix implantation. To date, the choice of knee cartilage treatment is

guided by patient age, goal, and expectations, the association of other joint tissue injuries, history of prior treatment, and the cartilage defect dimension (extent, size, and depth) and location. Although not routinely performed, arthroscopic biopsy is still considered the gold standard to assess cartilage repair tissue quality in cartilage repair. However, due to the associated morbidity of arthroscopy, MRI became the most widely used tool to assess the status of repair tissue. The radiologist must be aware of "normal" findings associated with these procedures, as well as "abnormal" findings, which may require short-term follow-up or therapeutic intervention.

Repair tissue morphology on MRI strongly depends on the surgical technique. Hence, concise clinical information from the referring physician is critical for a comprehensive and accurate radiological assessment. Generally, MR imaging of cartilage repair in the knee should be performed with dedicated extremity coils. While examinations during the clinical routine are usually performed on 1.5 T and 3 T systems, a considerable number of studies have already been carried out on 7 T systems. The higher SNR that is offered by high-field and ultrahigh-field MR is invested in faster acquisitions or higher spatial resolution which is crucial in cartilage imaging [50, 51]. Generally, an in-plane resolution of 0.3 mm or less is favored to enable an adequate and reliable display of the fraying of cartilage [19].

14.2.4.1 Marrow Stimulation

Post bone marrow stimulation surgical procedure, the repair tissue undergoes a gradual maturation process that is well reflected by MR morphology. Soon after microfracture surgery, the creation of tiny fractures in the underlying subchondral bone results in the development of a super-clot, which fills the defect region. This initial phase involving genesis of repair tissue appears hyperintense on T2W images compared to adjacent healthy cartilage. In this early phase, even differentiation from fluid can be challenging [52], which emphasizes the importance of additional clinical information for adequate radiological assessment. As the pluripotent bone marrow cells infiltrate to the defect site and differentiate, the repair tissue consolidates. Usually, the clot takes about 8–15 weeks to be replaced by fibrous-like tissue and about 4 months postsurgery to form fibrous or fibrocartilage repair tissue. Concomitantly, the MR signal intensity decreases continuously until it is similar to or even lower than that of healthy cartilage [53, 54]. The higher the fibrous component of the repair tissue, the lower the MR signal compared to the adjacent native articular cartilage. This maturation process should normally be completed after 1–2 years, with the repair tissue filling the former defect and developing an even surface. In the early postoperative phase, bone marrow edema is frequently observed but should gradually resolve over time. However, persistent bone marrow edema may be a sign of treatment failure [52, 53].

14.2.4.2 Osteochondral Autograft and Allograft Transfer

Osteochondral auto- and allograft transfers are valuable treatment alternatives to address cartilage injury [3]. In osteochondral autograft transplant (OAT), OC plugs are harvested from low-weight-bearing areas of the knee and transferred into the cartilage lesion site. Naturally, the size of treatable defects (usually up to 2.5 cm^2) is limited by the amount of available OC donor tissue [55]. In comparison, allograft procedure involve obtaining OC plugs from donor knee with the advantage that it does not create additional OC lesions at the donor site of the patients knee. Therefore, allograft procedure can also be used to cover larger cartilage defects. Regarding the radiological follow-up, the main difference between the two techniques relates to an imperative additional MR assessment of donor sites after osteochondral autograft.

MR Image analysis should include the evaluation of the number and size of the OC graft, the contour of the bone and cartilage interface, as well as an assessment of the MR signal of the graft, the donor site, and the adjacent bone marrow. Furthermore, contrast enhancement patterns and soft tissue abnormalities in the joint, such as joint effusion and synovitis, should be investigated. The OC grafts usually show solid, osseous

incorporation between 6 and 14 weeks. Initially, postsurgical subchondral bone marrow edema is often present but is expected to resolve as the graft incorporates into the subchondral bone. Normal fatty marrow MR signal is seen within and around the plugs when solid bony incorporation occurs. Poor integration of the graft with the adjacent native tissue may be suggested by cystic cavities shown as fluid-like high MR signal intensity on T2W images and persistent edema-like high MR signal within the subchondral bone marrow.

Several investigators have extensively described the postsurgical MR findings of the OC graft and the adjacent native tissue [56–58]. From these studies, the following normal findings and possible complications post OC graft can be derived: *normal* MR findings associated with OC autograft procedure include bone marrow edema in and around the grafts, which was noted in more than 50% of the subjects within the first 12 months [56]. The bone marrow edema persisted for up to 3 years in a small number of patients. Also of note was joint effusion and synovitis, which sometimes persisted for more than 2 years. Incongruities at the bone-bone interface were frequently found, while incongruities at the cartilage-cartilage interface were uncommon findings. These frequently observed substantial incongruities of the bone-bone interface might seem pathological at first; however, they should not be considered a complication. It is rather an inherent side effect of the technique due to the fact that the plugs are harvested in areas where the cartilage thickness may differ from the implant site. Since the surgeon aims for a smooth articular surface, the bone-bone interface may often be incongruent.

Complications of OC grafting may include graft loosening or migration, incongruency of the cartilage-cartilage interface and gaps between OC plugs and adjacent native cartilage. Although partial or complete necrosis of the grafts was noted, these represented relatively rare findings. In the study by Link et al. [56], OATS procedure in the knee was performed in 45 patients with one or more OATS cylinder implanted in each patient. Second-look arthroscopies and MRI findings consistent with osteonecroses were detected in six OATS cylinders. The osteonecrotic graft cylinders did not lead to the collapse of the bone or pathological changes of the cartilage. Interestingly, only two of these cases were associated with clinical abnormalities. An explanation might be that cartilage derives its nutrition almost exclusively from the synovial membrane, thus rendering its viability less interconnected with changes of this nature.

14.2.4.3 Cell-Based Repair Techniques

Similar to bone marrow stimulation techniques, the repair tissue matures over time after ACI, and matrix-associated chondrocyte transplantation (MACT) procedures. The maturation of repair tissue is documented by a decrease in MR signal intensity on T2W images. Initially the repair tissue appears hyperintense, but, over time, it develops a comparable MR signal intensity to that of healthy cartilage reference [52, 59, 60]. In the early postoperative phase, subchondral bone marrow edema is a normal finding, which should, however, gradually resolve during follow-up. Persistent bone marrow edema after 1 year might be indicative of (pending) treatment failure [52]. Similarly, incomplete integration on the border zones, as seen by thin fissure-like hyperintensities, is commonly observed at early stages but should also eventually resolve. What should be considered to be a defective fill in the early postoperative stage depends on the applied method. While slight underfill can be anticipated for MACT, complete fill or even overfill is commonly observed after ACI. However, both techniques should foster complete fill within 1–2 years. Subsequent graft hypertrophy is particularly associated with the use of periosteal flaps and might necessitate surgical debridement in symptomatic cases. Delamination is also more commonly observed with a periosteal cover than with synthetic collagen [61]. Graft delamination is best appreciated on T2W images and is characterized by a linear hyperintense signal that extends between repair tissue and underlying subchondral bone [52]. In most cases, the subchondral lamina should remain intact after ACI and MACT surgery.

14.2.5 Semiquantitative Scoring Systems of Cartilage Repair Based on Morphological Magnetic Resonance Imaging

Semiquantitative scoring systems play an important role in the postoperative evaluation of cartilage repair, as they allow for a standardized, reproducible, and objective assessment of defined parameters. This provides a mean to compare the outcome between different cartilage repair procedures and also compare results obtained from different studies. In particular, the Magnetic Resonance Observation of Cartilage Repair Tissue (MOCART) scoring system, in its original 2D design and in the updated 3D version, has been widely applied in research since its introduction in 2004 (refer to Chap. 13 and Appendix C). To facilitate the best repair tissue outcome for comparison between studies, the MOCART scores should be obtained at set time intervals. However, particularly in the early postoperative phase, these intervals may depend on the applied cartilage repair surgical technique. Despite their extensive use in research, the MOCART scoring system has not yet been fully integrated into the daily clinical routine. Since it is reasonable to hypothesize that this way of standardized reporting might also improve patient care in the daily routine, the integration of MOCART scoring system is highly encouraged.

14.2.5.1 Magnetic Resonance Observation of Cartilage Repair Tissue

The original MOCART [62] assessed and scored [59] nine different variables: filling of the defect, integration with adjacent cartilage and bone, surface of the repair tissue, structure of the repair tissue, signal characteristics of the repair tissue, subchondral lamina at the repair site, subchondral bone at the repair site, the presence of adhesions, and synovitis. These variables were evaluated on the basis of several 2D sequences acquired with a circular polarized knee coil and a high-resolution sagittal dual FSE sequence acquired with a surface coil [62]. In the MOCART, zero to a hundred points may be reached, with zero representing the worst and one hundred the best radiological outcome possible [59]. The MOCART can be employed for the assessment of any type of cartilage repair technique and its versatility is evidenced by its extensive use in research in both cross-sectional and longitudinal studies [63].

14.2.5.2 Three-Dimensional Magnetic Resonance Observation of Cartilage Repair Tissue

Subsequently, high-resolution, isotropic 3D sequences were developed, which enabled isotropic image acquisitions with a voxel size down to 0.4 mm. Using multi-planar reconstruction, these data sets can be reconstructed in every plane without a loss of resolution. Welsch et al. used this new possibility to establish and introduce the 3D-MOCART, a variation of the original MOCART which is based on the acquisition of a single, isotropic 3D sequence [64]. For that purpose, the authors chose the 3D True-FISP, a gradient echo-based sequence. Taking advantage of the smaller slice thickness and the possibility of reformatting any desired image plane, the authors extended the score to a total of 11 variables. The 3D MOCART also assesses the three-dimensional position of the repair tissue and its borders with healthy cartilage reference in every plane. Furthermore, the authors introduced the possibility to denote the relative 3D position of some features. The nine variables that were assessed in the original 2D-MOCART showed good correlation with the 3D-MOCART [64]; however, there was a larger number of artifacts in the 3D-True-FISP compared to the 2D sequences. Subsequently, a different 3D sequence, the turbo spin echo-based 3D-SPACE, was evaluated for its usability in assessing the 3D-MOCART [65]. In this study, the 3D-SPACE sequence was compared to the 3D True-FISP, as well as the 2D sequences. The authors concluded that, although different 3D sequences may be used to determine the 3D-MOCART score, the 3D-SPACE yielded the best results. However, despite the creation of the 3D MOCART, the traditional MOCART based on 2D sequences is still widely used.

14.2.5.3 Cartilage Repair Osteoarthritis Knee Score

The MOCART scoring system allows for objective and reproducible assessment of repair tissue and its surrounding structures. However, it does not take into account the condition of other structures of the knee such as meniscus, ligament, tendon, etc. The condition of these structures might have a profound impact on the clinical presentation and outcome. In addition, their assessment is a prerequisite for an investigation of whether it is possible to delay or prevent OA development after cartilage injury. The Cartilage Repair OA Knee Score (CROAKS) [66] combines the features assessed in the MOCART with features from the Magnetic Resonance Imaging Osteoarthritis Knee Score (MOAKS) [67], with the goal of assessing not only the repair site but also the joint in its entirety, to foster a more holistic view. The CROAKS can be used for the assessment of all different types of repair procedures.

14.2.6 Summary of Magnetic Resonance Morphological Imaging of Cartilage Repair

Fast spin echo and GRE sequences are the cornerstone of knee MRI. For quantitative imaging, isotropic 3D-GRE sequences, such as 3D-FLASH or 3D-DESS, are utilized. Whereas morphological MRI for cartilage evaluation has focused on qualitative features thus far, a quantitative approach may yield even more information. For this purpose, standardization is important both during the acquisition of images (i.e., scanners, sequences, and patient-specific factors) and during the further processing of images (i.e., volume of interest identification, segmentation, and definition, extraction, and qualification of parameters).

For cartilage repair, high-resolution MRI provides an accurate, noninvasive evaluation of the repair site and provides the basis for the use of scoring systems, such as the MOCART score, which enables an evaluation of the development of the cartilage repair site over time and facilitates interindividual comparison. Particularly in patients after matrix-associated autologous chondrocyte transplantation, dynamic processes with biological cartilage repair can be observed over time. Thus, post cartilage repair surgical procedure, two follow-up MR examinations in the patient without clinical symptoms seem to be appropriate, the initial MR assessment after the first year and subsequently after the second year. Whenever clinical symptoms develop or a new trauma occurs, follow-up MR examination should be performed immediately.

14.3 Biochemical Magnetic Resonance Assessment of Cartilage Repair Tissue

To visualize the constitution of articular cartilage and cartilage repair tissue, a variety of different methodologies are available. These methodologies should depict either one or a combination of the different components of healthy hyaline articular cartilage. Chapter 1 describes in depth the structure, morphology, and composition of articular cartilage at the macro- and microlevel.

Articular cartilage is a complex, dense, specialized connective tissue that relies on the diffusion of solutes for its nutrition [68]. Responsible for the biomechanical properties of articular cartilage is the extracellular matrix, mainly composed of water (~75%), collagen (~20%), and proteoglycan aggregates (~5%) [68, 69]. Water either freely moves throughout the matrix or is bound to macromolecules. Collagen is largely represented by type II, which creates a stable network throughout the cartilage. Proteoglycans are composed of a central core protein with glycosaminoglycan (GAG) side chains which carry up to two anionic groups on its disaccharide units, which contribute to a negative charge of the cartilage matrix. As these ionic groups are fixed to the extracellular matrix components, they are referred to as *fixed charge*, and their distribution within the tissue is described as *fixed charge density (FCD)* [70–72]. This negative FCD attracts positive ions and water molecules, which strongly contribute to the unique mechanical properties of articular cartilage. Articular cartilage architecture

is stratified primarily according to the orientation of collagen within a three-dimensional network [69, 73]. The superficial/tangential zone is characterized by flattened chondrocytes, relatively low quantities of proteoglycans, and high quantities of collagen fibrils arranged parallel to the articular surface. The middle/transitional zone has round chondrocytes, a high level of proteoglycans, and a random arrangement of collagen fibers. The deep/radial zone is characterized by low cell density, thick collagen fibrils that are perpendicular to the bone, and columns of chondrocytes. After the "tidemark," the underlying calcified cartilage layer is partly mineralized and acts as the transition zone between cartilage and the subchondral bone.

The structure and the components of healthy hyaline cartilage form the basis for the different biochemical MR methodologies and their use in the evaluation of articular cartilage in disease and repair. Many of these approaches have already been successfully applied for the assessment of cartilage repair. Depending on the different cartilage repair techniques, the cartilage repair tissue in histological studies has appeared to be hyaline-like cartilage, mixed hyaline-like and fibrocartilage, fibrocartilage or fibrous. Nevertheless, these histological studies show different results for these different cartilage repair procedures [74–81].

Since changes in GAG content generally take place before changes in collagen architecture occur, depiction of the ultrastructure of the repair tissue, using biochemical MRI, may be important not only to detect different stages of cartilage degeneration (GAG decrease) but also to detect different stages of cartilage repair (GAG increase). Negatively charged proteoglycans, composed of a central core protein with bound GAG chains, have been visualized by delayed gadolinium-enhanced MRI of cartilage (dGEMRIC) [82], sodium MR imaging [83, 84], and more recently, chemical exchange-dependent saturation transfer (CEST) [85, 86]. To date, only dGEMRIC was introduced into clinics for cartilage repair imaging; however, recently linear gadolinium contrast agents have been withdrawn from the market due to the deposition of gadolinium in the brain [87]. As such, based on the decision of the European Medical Agency, the clinical use of dGEMRIC is now severely restricted.

Although, also reflective of water content, the classic biochemical MR method that focuses on the collagen content and architecture of articular cartilage is transverse relaxation time (T2) mapping [86, 88, 89]. In addition to the T2 of articular cartilage, recently, T2* relaxation was shown to reflect collagen architecture and could be a promising tool for faster detection of tissue degeneration and repair tissue assessment within shorter acquisition times and higher resolutions [89–95]. Furthermore, magnetization transfer contrast (MTC) might also play a more important role in future cartilage imaging approaches. Another MR technique reported to reflect a combination of cartilage macromolecules, namely the proteoglycan [96] plus collagen content of articular cartilage [97], might be T1ρ relaxometry.

14.3.1 T2 Relaxation Time Mapping

The T2 of articular cartilage is a sensitive parameter for the evaluation of changes in water and collagen content, as well as tissue anisotropy [88]. Cartilage T2 reflects the interaction of water and the extracellular matrix on a molecular level, with the collagen fiber orientation defining the layers of articular cartilage. The 3D organization and the "gothic" arch-like curvature of the collagen network, influenced by water mobility, the proteoglycan orientation, and the resulting magic angle at 55° (with respect to the static magnetic field), influence the appearance of T2 [73, 98]. In healthy articular cartilage, an increase in T2 values from deep to superficial cartilage layers can be observed, based on the anisotropy of collagen fibers running perpendicular to cortical bone in the deep layer of cartilage [99]. Latter orientation reduces the mobility of water protons with consecutive lower T2 relaxation times. Histologically validated animal studies have shown this zonal increase in T2 values to be a marker of hyaline or hyaline-like cartilage structure after cartilage repair procedures in the knee [100, 101]. To visu-

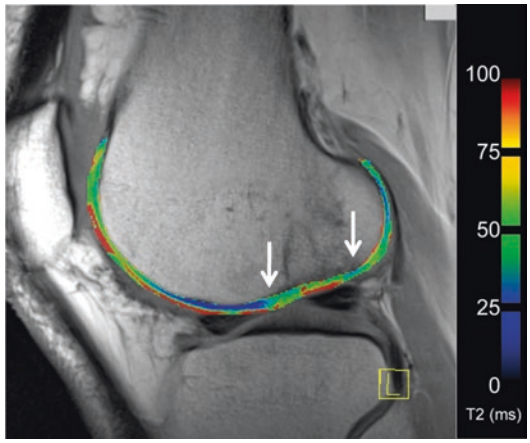

Fig. 14.6 Sagittal multi-echo spin-echo MR image with a color-coded T2 map overlay of the lateral femoral condyle of a 32-year-old male, 6 months after matrix-associated chondrocyte transplantation. Higher T2 values within the repair tissue (arrows) can be appreciated, when compared to the surrounding native articular cartilage. (Acquisition parameters: TR: 1650 ms; TE: 12.9, 25.8, 38.7, 51.6, 65.5, 77.4; flip angle 180°; matrix size: 384 × 384; FOV: 16 cm; slice thickness: 3 mm; slices: 6; TA: 5:37 min)

alize this zonal variation in vivo, high spatial resolution is essential, which can already be achieved at high-field MR, together with dedicated multichannel coils in clinical approaches [102] (Fig. 14.6). In addition, as shown in a comparison of T2 mapping at 3 T and 7 T, the SNR also benefits from the increased field strength [103]. As a result, with the appropriate technological setup, even in joints with thin cartilage layers such as the ankle, a zonal evaluation of cartilage is possible [102], and also the differences in cartilage T2 values of distinct anatomical regions, such as between the ankle and knee, can be quantified [104].

Recently, it has been observed that T2 mapping may provide valuable information about the development and progression of OA [105–108]. In a study with data from the OA Initiative, the authors found increased T2 values in knees, which progressed from a Kellgren-Lawrence (KL) score of 0 to a KL of 2 within 4 years compared to controls without progression [109]. Another study found a positive correlation between the ICRS grade of cartilage and increased T2 values next to the defect [110]. Further applications of T2 mapping may include the monitoring of cartilage alterations in the course of ACL injury and reconstruction, as higher T2 values prior to ACL reconstruction correlate positively with the clinical outcome 1-year postsurgery, according to the Knee Injury and OA Outcome Score [111]. In 2016, an initial randomized controlled trial used T2 values to evaluate the effects of a physical exercise intervention in early OA [112]; there was a decrease of T2 values after 4 months of aquatic training in postmenopausal women with early OA. This promising research must be further analyzed to determine the specific role of T2 as an absolute quantification parameter.

In cartilage repair tissue, global (bulk) T2 values, as well as line profiles, have shown an increase in the early postoperative follow-up, which might enable visualization of cartilage repair maturation [113]. Furthermore, another study has shown the ability of zonal T2 evaluation to differentiate cartilage repair tissue after microfracture (MFX) and MACT [27]. Whereas cartilage repair tissue after MFX, histologically seen as fibrocartilage, has shown no zonal T2 value increase from deep to superficial cartilage aspects in the mentioned study, repair tissue after MACT, histologically reported as hyaline-like, has shown a significant cartilage stratification.

The advance of ultrahigh magnetic field strengths enables the application of higher spatial resolution and, thus, an improvement in T2 mapping through better visualization of zonal variations in cartilage [103]. However, higher field strengths introduce disadvantages, such as a higher specific absorption rate (SAR) and B1 inhomogeneity. This affects common sequences for the derivation of T2 maps (e.g., Carr-Purcell-Meiboom-Gill or CPMG) and renders their application challenging. An alternative is to compensate for these issues by using single-echo spin echo (SE) sequences but with the disadvantage of an increase in acquisition time [114]. A possible solution is provided by the triple-echo steady-state (TESS) sequence [115] (Fig. 14.7). This new SSFP sequence acquires three echoes in one repetition time (TR) and has an inherent sta-

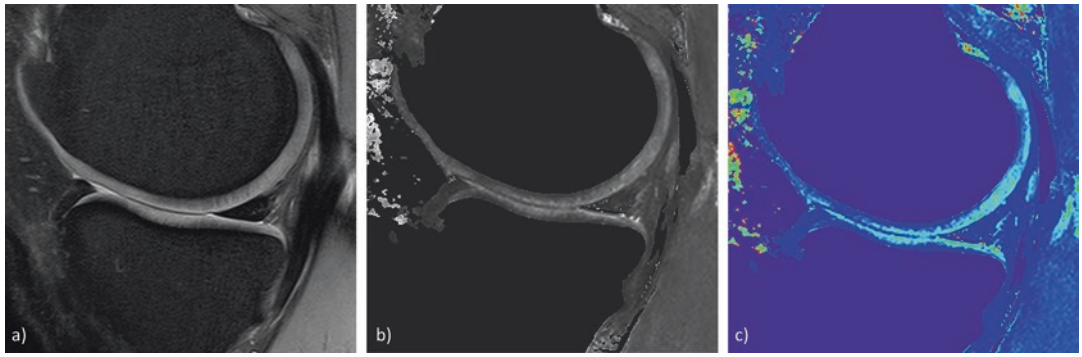

Fig. 14.7 Proton density-weighted 7 T MRI of the medial compartment femoro-tibial articular cartilage of a 26-year-old healthy male volunteer. Three cartilage layers can be seen from the bone-cartilage interface to the cartilage surface. The hypointense lines perpendicular to the bone seem to resemble the effects of the underlying collagenous architecture (**a**). T2-map calculated from a 3D triple-echo steady state (3D–TESS) sequence at 7 T (acquisition time = 1:48 min) from the same subject, where hyperintense voxels highlight the distribution of T2 values throughout the cartilage. Again, three layers can be differentiated (**b**). The same T2-map with different coloring scheme to better visualize the T2 value distribution within articular cartilage revealed brighter voxels having a higher T2 value (**c**)

bility against B1 inhomogeneity. In addition, due to low flip angles, TESS makes it easier to adhere to the SAR limit, thus further increasing the synergistic value of TESS and ultrahigh-field strengths. In total, the image acquisition can be accelerated by a factor of 4 to 5 compared to conventional multi-echo, multi-slice spin echo sequences (CPMG) used for T2 mapping [116, 117].

14.3.2 T2*(Star) Relaxation Time Mapping

Compared to T2 values, T2* additionally reflects very short transverse de-phasing effects caused by local field heterogeneities due to static magnetic field inhomogeneities, applied gradients, chemical shift, and magnetic susceptibility – at the macroscopic level, at the cartilage bone interface, or at the microscopic level within the cartilage ultrastructure [90, 118, 119]. Since SE sequences eliminate these de-phasing effects by applying refocusing pulses, T2* acquisition is exclusive to GRE sequences because refocusing is performed by magnetic gradients instead [118, 119]. Moreover, T2* relaxation is less influenced by stimulated echoes and magnetization transfer [120].

T2* maps are created similar to T2 maps: for each slice, several images are acquired with multi-echo sequence protocols at set echo times and are used to fit the signal levels to the corresponding echo time (TE) by applying a mono- or bi-exponential decay equation [121]. No special hardware components are needed for T2* mapping and further featured benefits are a biochemical approach with high-resolution 3D acquisition within short scan times [122]. Because the deep and calcified zone of articular cartilage consists of highly organized, dense collagen fibrils, sequences that are able to acquire short TEs provide more information and are more sensitive to pathological changes at this specific location [93, 118, 122]. With ultrashort TE (UTE) T2* mapping, acquisition of echo times on the order of 0.3 ms is possible. This allows the evaluation of higher organized tissues more sensitively, especially by omitting longer TEs that are related to cartilage bulk water content, underlining the potential ability and robustness of this method to improve the assessment of articular degeneration [91, 118, 123].

Due to its sensitivity to changes in collagen architecture, T2* mapping was investigated as another possible modality for cartilage repair tissue evaluation. Studies have demonstrated and histologically validated a decrease in T2* relax-

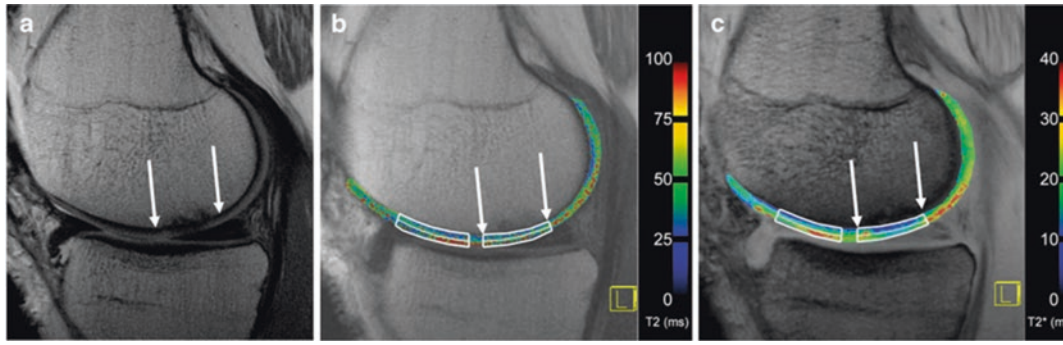

Fig. 14.8 MRI of the medial femoral condyle of a patient obtained at 60 months after matrix-associated chondrocyte transplantation. MR images were obtained using morphological proton density Turbo Spin Echo (PD-TSE) sequence (**a**), matched quantitative T2 map (**b**), and T2* (**c**) maps. Arrows mark the area of cartilage repair. The rectangular regions of interest (ROIs), considering a possible zonal variation, provided information on the mean (full-thickness) as well as the deep and superficial aspects of control native cartilage (left) and cartilage repair tissue (right, arrows). Zonal stratification is visible for both T2 and T2* images in most parts of the cartilage. A possible "magic angle" effect occurs within the posterior aspect of the femoral condyle. Lower T2* values and similar T2 values within the cartilage repair tissue are apparent, compared with the adjacent cartilage (These images are reproduced with permission from: Welsch et al. [125])

ation time measurements with increasing grades of cartilage degeneration and its sensitivity to mild and severe degradation [91, 94, 124]. In a retrospective study, the initial in vivo measurements in patients who previously underwent MACT were also successful at 2.5 years postsurgery in depicting similar global T2 and T2* values in the superficial and deep layer of healthy, native cartilage as well as repair tissue. Furthermore, a zonal stratification of signal intensity values, with values increasing from the depth to the surface, was shown for healthy cartilage, but not within the MACT repair tissue [90]. A prospective follow-up with examinations at 3, 6, 12, 24, 36/42, and 60 months post-MACT demonstrated comparable T2 values between repair tissue and healthy cartilage but lower T2* in repair tissue. The zonal differences in T2* values were also more pronounced compared to T2 (Fig. 14.8) [125]. Another study that evaluated MFX at 1.9 years after surgery found higher and positively correlated T2 and T2* values in healthy cartilage compared to repair tissue. Spatial variation from deep to more superficial layers was again demonstrated within healthy cartilage but not in MFX repair tissue [93].

Although these results suggest promising future applications for a faster isotropic, biochemical imaging modality, more studies need to be performed to create normative data and establish standardized acquisition protocols.

14.3.3 T1rho Magnetic Resonance Imaging

Relaxation time in the rotating frame (T1rho also called T1ρ) is a time constant with elements of both T1 and T2 weighting, and it characterizes magnetic relaxation of spins under the influence of a radiofrequency field that is parallel to the magnetization. The resulting contrast is sensitive to the low-frequency interactions between water molecules and their local macromolecular environment, such as collagen and GAGs. The amount of their respective macromolecular contribution, however, is still under discussion. Regatte et al. observed changes in T1ρ in cartilage plugs that were chemically or enzymatically depleted of GAG, but not in collagenase-treated tissue [126], suggesting a sensitivity to GAG content. However, Menezes et al. found no correlation between the cartilage $T_1\rho$ and GAG concentration [127]. In addition, it has been reported that the dominant T1ρ and T2 relaxation mechanism at B_0 (=static magnetic field) < 3 T is a dipo-

lar interaction due to slow anisotropic motion of the water molecules in the collagen matrix [97]. This fits the observation that, similar to T2 measurements, T1ρ is also influenced by collagen orientation, as evidenced by the presence of the magic angle effect. These findings were reinforced by a study that compared T1ρ and dGEMRIC with histology and concluded that T1ρ is not suitable to accurately measure GAG content in vivo in OA patients [128]. However, even though T1ρ does not seem to reflect a specific macromolecular component of the extracellular matrix exclusively, it has been demonstrated to be a predictive marker for the development of morphologic lesions in articular cartilage [129]. T1ρ has also been used in addition to T2 relaxation time measurements to monitor repair tissue maturation after MFX and mosaicplasty by Holtzman et al. [130]. The authors concluded that T1ρ and T2 relaxation time measurements are complementary methods. A study investigating patients after MFX [131] noted a significant difference in both T1ρ and T2 between repair tissue and healthy reference cartilage after 3–6 months. At the 1-year follow-up, only T1ρ still demonstrated a significant difference. Based on these results, the authors concluded that T1ρ is also suited for the noninvasive evaluation of cartilage repair tissue.

14.3.4 Magnetization Transfer Contrast

The use of MTC imaging for articular cartilage was first described by Wolff et al. [132]. MT effects are based on the interaction of two different water pools, a free (unbound) bulk water pool, which is visible by MRI, and a bound water pool, with water molecules bound to macromolecules. The mobility of these bound water molecules is decreased to such an extent that, with standard MRI, protons of these water molecules do not provide a measureable MR signal. In certain tissues of the human body, such as the liver, thyroid, muscle, and cartilage, however, there is an interaction between the two pools: either chemical exchange or exchange of magnetization due to a dipolar interaction (so-called cross-relaxation). After saturation of bound water protons by off-resonance pulses, the magnetization of the free water pool is also affected, resulting in a reduction of the observable magnetization, which is reflected on MR image as reduced signal intensity. Thus, MT is tissue-specific and may provide a quantitative method for tissue characterization of basic macromolecular dynamics and chemistry [132–137]. Nevertheless, to date, MT has rarely been used for the quantitative in vivo evaluation of articular cartilage. However, one study demonstrated initial, and promising, results for cartilage repair [138]. Using a magnetization transfer-sensitized, SSFP MRI sequence introduced by Scheffler and Bieri [139], MTC was compared to T2 mapping for the assessment of global mean values, as well as for zonal variations of healthy, native articular cartilage and repair tissue after MACT and MFX [140]. Significant differences in global mean MT ratio (MTR) values were observed between sites of healthy cartilage and that of cartilage repair. The decrease in MTR was more pronounced in post-MFX repair tissue compared to post-MACT repair tissue. However, in contrast to T2 relaxation, MTC showed lower values for both MFX and MACT, whereas T2 showed lower values only for MFX, when the repair tissue was compared to surrounding healthy, native cartilage. Hence, both biochemical methods do not measure exactly the same properties of native cartilage and repair tissue. Considering the results of in vitro studies [141, 142], it seems that collagen concentration and collagen orientation may possibly play the most important role for both MTC and T2 relaxation. The latter, nevertheless, might also be influenced by hydration, to which MTC might be less sensitive.

When using these (and other) biochemical MR techniques in cartilage repair, one of the most important things is to either (i) use an area of healthy cartilage as an internal reference or (ii) perform longitudinal studies and compare the same subject at the same time of day. Furthermore, histologically validated studies might help to further clarify the impact of biochemical MR techniques in the visualization of cartilage

ultrastructure and specific macromolecular components of articular cartilage.

14.3.5 Glycosaminoglycan Chemical Exchange Saturation Transfer

Glycosaminoglycan chemical exchange saturation transfer (gagCEST) is another promising technique for the noninvasive evaluation of glycosaminoglycan (GAG) content in articular cartilage in vivo [85]. GagCEST imaging exploits the fact that, in articular cartilage, labile protons from the OH groups of GAGs are in constant exchange with the protons of water molecules. Similar to MTC experiment, these labile protons on GAGs can be saturated using radiofrequency-selective saturation pulses. When these protons are then subsequently transferred to the bulk water pool by chemical exchange, they reduce the bulk water signal, which can, in turn, be measured. By applying this saturation over a longer period, saturated protons accumulate in the water pool, thus providing a significant contrast enhancement [143]. Due to the intricacy of the method, however, the quality of gagCEST maps is prone to error by a variety of factors, such as B0 and B1 inhomogeneities, motion artifacts, varying labeling efficiency, as well as insufficiently accurate definition of the z-spectra. In 2011, Schmitt et al. [144] investigated patients after MFX and MACT using gagCEST, at a mean follow-up time of 21 months, and compared the results to those reported with sodium imaging at 7 Tesla (Fig. 14.9) [144]. These investigators found lower asymmetric magnetization transfer ratio (MTR_{asym}) values in repair tissue than in healthy reference cartilage and observed a strong correlation between gagCEST and sodium imaging, indicative of the specificity of gagCEST for GAGs. GagCEST was also used to assess the outcome of autologous OC transplantation in nine patients after a mean follow-up of 7.9 years, along with sodium imaging at 7 T and T2-mapping at 3 T [145]. The clinical patient outcome was good, as demonstrated by a median, modified Lysholm score of 90. The strongest correlation was observed between gagCEST and sodium imaging ($\rho = 0.952$ with a 95% confidence interval of [0.753; 0.992]). However, only T2-mapping showed a correlation with the modified Lysholm score.

Due to rather long measurement times, patient motion is an important issue that should be addressed both mechanically, via good fixation and via post-processing, with registration tools [146]. Currently, the best results are obtained on ultrahigh-field systems [147] because of the

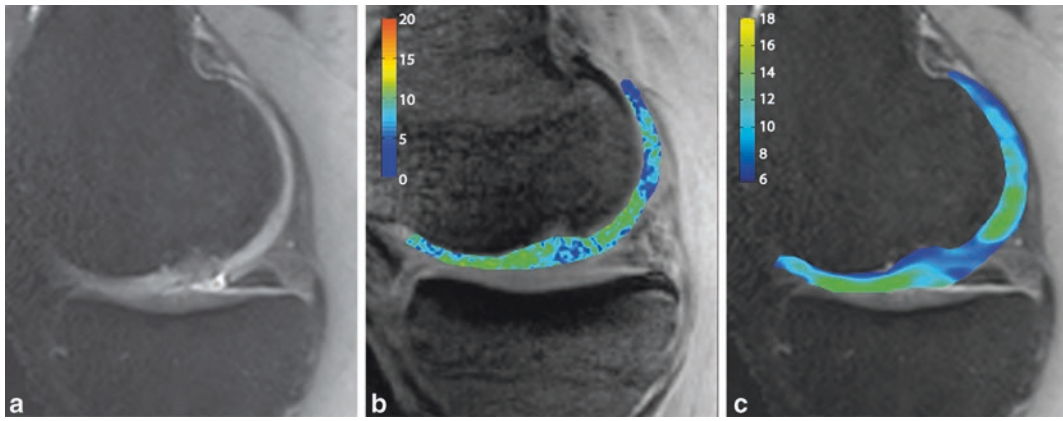

Fig. 14.9 A 30-year-old patient after microfracturing in the medial femoral condyle was examined using high-resolution (**a**) morphological, (**b**) gagCEST, and (**c**) 23Na MR imaging. Color bars on (**b**) and (**c**) represent MTR asym values summed over offsets from 0 to 1.3 ppm (gagCEST) and sodium SNRs, respectively. Both techniques show decreased signal intensity in repair tissue compared with surrounding native tissue (With permission from Ref. [144])

higher signal-to-noise ratio and spectral resolution compared to routine 3 T systems [148]. Conversely, B_0 (static magnetic field) and B_1 (radiofrequency field strength) inhomogeneities, as well as SAR limitations, are more pronounced at ultrahigh fields. In particular, accurate B_0 correction has been shown to be crucial for accurate gagCEST measurements [147]. For that purpose, water saturation shift referencing (WASSR) [149] was introduced and was shown to further improve the quality of gagCEST maps [150]. Despite these challenges, gagCEST has valuable advantages. Unlike dGEMRIC, the gagCEST imaging does not require the administration of a contrast agent but rather employs the endogenous contrast provided by chemical exchange. In addition, gagCEST does not rely on special multinuclear hardware as does sodium imaging. Furthermore, gagCEST combines GAG specificity with favorable spatial resolution. However, additional refinement will be necessary to make this technique applicable for routine clinical assessment.

14.3.6 Delayed Gadolinium-Enhanced Magnetic Resonance Imaging

Glycosaminoglycans are important for the biochemical and biomechanical behavior of cartilage tissue. GAGs are the main source of fixed charge density in cartilage and are often decreased in the early stages of cartilage degeneration [151] or in cartilage repair tissue [152]. Intravenously administered gadolinium diethylenetriamine pentaacetate anion (Gd-DTPA^{2-}) penetrates the cartilage through both the articular surface and the subchondral bone. The contrast equilibrates in inverse relation to the FCD, which is, in turn, directly related to the GAG concentration. Therefore, T1, which correlates inversely with the Gd-DTPA^{2-} concentration, becomes a specific measure of tissue GAG concentration, suggesting that Gd-DTPA^2-enhanced MRI has the potential to monitor the GAG content of cartilage in vivo [153]. Thus, T1 mapping, enhanced by delayed administration of Gd-DTPA^{2-} (T1 dGEMRIC), was considered the most widely used methodology to detect proteoglycan depletion in articular cartilage (especially in the knee) and has shown promising results [154, 155]. However, there are several drawbacks that hamper the clinical applicability of dGEMRIC due to a costly protocol in terms of time. Further, there are risks in the form of nephrogenic systemic fibrosis, as well as the not-yet-completely-understood retention of gadolinium deposits in tissue [156]. Considering the necessary double dose of Gd-DTPA^{2-} for dGEMRIC [82], special caution is warranted.

As differences in pre-contrast values between repair tissue and normal hyaline cartilage are larger compared to early cartilage degeneration, the pre-contrast T1 values must be calculated in cartilage repair tissue as well [152]. The concentration of GAG is represented by delta $\Delta R1$, i.e., the difference in relaxation rate ($R1 = 1/T1$) between $T1_{precontrast}$ and $T1_{postcontrast.}$ Thus, the sequence must be performed twice, for pre-contrast and delayed post-contrast T1 mapping. This increases the total scan time and requires a break between the two MR scans, in which the contrast agent must be administered. A delay of at least 90 min after injection is then required for penetration of the contrast agent into the cartilage. Scan time reduction, compared to the standard inversion recovery (IR) evaluation, has been achieved with a different approach using fast T1 mapping [157]. Although the 90-min delay is still required, this might increase the clinical applicability of the dGEMRIC technique.

Using dGEMRIC, one study was able to differentiate between different postsurgical technique repair tissues with higher delta $\Delta R1$ values, and thus, lower GAG content, in cartilage repair tissue after MFX, compared to MACT [158]. Furthermore, dGEMRIC may help to determine alterations associated with the development of OA, both in hip dysplasia and femoroacetabular impingement [159, 160], as well as in the longitudinal evaluation of knee cartilage [161, 162]. The applicability of this technique has also been shown in regions other than the knee and hip joint [163–165].

14.3.7 Sodium Magnetic Resonance Imaging

In articular cartilage, positive sodium ions are the naturally distributed counterions to the negative fixed charged density, which is mainly caused by negatively charged side chains of GAGs. This direct proportionality allows indirect estimation of the concentrations and distributions of GAGs in articular cartilage through the assessment of relative sodium concentrations [166–169]. Although sodium (^{23}Na) is the second best detectable nucleus in living systems, sodium imaging is challenging due to short T2 relaxation times and the significantly lower concentration of sodium as compared to water protons in articular cartilage. These properties result in low intrinsic SNR, which makes sodium MRI a technically challenging, especially in a clinical environment with limited scan times [170–174]. These challenges were addressed with the development and introduction of dedicated coils and new sequences that made sodium measurements more feasible, even in a clinical setting [174]. Moreover, it was reported that sodium imaging is comparable to T2 mapping with regard to repeatability and, in addition, might provide sufficient sensitivity for the in vivo evaluation of OA [175]. However, compared to proton imaging, sodium imaging is still limited by resolutions between 2–4 mm and longer scan times (15–30 min), the requirement for special hardware with a multinuclear setup, the need for dedicated coils – as well as favorable 3D sequences with very short TEs – and, especially, by the need for higher field strengths (3 T or, better, 7 T) [176, 177].

Since GAG depletion precedes collagen deterioration and the resultant gross morphological damage, one of the great potentials sodium imaging carries is its ability to detect pathological changes early, before they become visible on morphological MR images [178–180]. Early clinical trials for OA evaluation concluded that sodium imaging may be useful for diagnosing and monitoring early changes in the GAG content of OA cartilage [181, 182]. As partial volume effects play an important role because of the previously mentioned limited resolutions, the sodium signal may be contaminated by synovial fluid or joint effusion [182]. With further technical refinements, such as IR preparation-based fluid suppression, it was possible to report that sodium was a reliable and reproducible biomarker for the prediction of OA [183, 184]. The sensitivity of this method was demonstrated in a clinical trial on patients suffering from type 1 diabetes mellitus (DM1) without any pathological findings based on clinical examination or morphological MR imaging in the knee. Sodium imaging, however, already revealed slight biochemical changes in articular cartilage composition in these DM1 patients compared to healthy volunteers [185].

The first sodium imaging studies on characteristics of repair tissue demonstrated the ability of this technique to successfully discriminate repair tissue from native cartilage after MACT or MFX surgical techniques for treatment cartilage repair. Furthermore, high correlations of these particular findings to dGEMRIC, as well as to gagCEST values, were also shown (see also Fig. 14.9) [144, 186]. Based on these results, the assessment of the value of sodium imaging in evaluating the quality of repair tissue in bone marrow stimulation (BMS) and MACT was performed. Although the morphological appearance of the repair tissue evaluated by the MOCART score showed no significant difference, higher sodium MR signal intensities, indicative of higher GAG concentration, and thus a higher quality of repair tissue were observed in patients who underwent MACT. This suggests that sodium MRI could be used not only as a marker for postsurgical follow-up but also as a possible noninvasive method for performance evaluation of new cartilage repair surgical techniques, at least in the knee [187].

Overall, sodium imaging is a promising, reproducible, and sensitive approach for the noninvasive assessment of cartilage composition. However, in order to confirm the clinical feasibility, hardware and software optimization must be performed to ameliorate current limitations, such as limited spatial resolution, relatively long scan times, and restriction to higher field strengths.

14.4 Conclusions

Magnetic resonance imaging has made tremendous advances over the last several years and has matured into the most commonly used noninvasive tool for the assessment of cartilage injury, degeneration, and repair. Both morphological imaging (with the use of semiquantitative scores or volumetric measurements) and biochemical imaging can provide quantitative, reproducible data. These data have been shown to have the potential for the early diagnosis of degeneration and injury, as well as for treatment monitoring. Thus, both morphological and biochemical imaging form one of the cornerstones in the current attempts aimed at the success of surgical cartilage repair techniques and improving OA therapy.

References

1. Curl WW, Krome J, Gordon ES, Rushing J, Smith BP, Poehling GG. Cartilage injuries: a review of 31,516 knee arthroscopies. Arthroscopy. 1997;13(4):456–60.
2. Buckwalter JA, Mankin HJ. Articular cartilage .2. Degeneration and osteoarthrosis, repair, regeneration, and transplantation. J Bone Joint Surg Am. 1997;79A(4):612–32.
3. Hunziker EB, Lippuner K, Keel MJ, Shintani N. An educational review of cartilage repair: precepts & practice–myths & misconceptions–progress & prospects. Osteoarthritis Cartilage. 2015;23(3):334–50.
4. Buckwalter JA. Evaluating methods of restoring cartilaginous articular surfaces. Clin Orthop Relat Res. 1999;367:S224–S38.
5. Roberts S, McCall IW, Darby AJ, Menage J, Evans H, Harrison PE, et al. Autologous chondrocyte implantation for cartilage repair: monitoring its success by magnetic resonance imaging and histology. Arthritis Res Ther. 2003;5(1):R60–73.
6. Gersoff WK. Considerations prior to surgical repair of articular cartilage injuries of the knee. Oper Tech Sports Med. 2000;8(2):86–9.
7. Alparslan L, Minas T, Winalski CS. Magnetic resonance imaging of autologous chondrocyte implantation. Semin Ultrasound CT MR. 2001;22(4):341–51.
8. Winalski CS, Minas T. Evaluation of chondral injuries by magnetic resonance imaging: repair assessments. Oper Tech Sports Med. 2000;8(2):108–19.
9. Peterfy CG, Majumdar S, Lang P, Vandijke CF, Sack K, Genant HK. Mr-imaging of the arthritic knee – improved discrimination of cartilage, synovium, and effusion with pulsed saturation-transfer and fat-suppressed T1-weighted sequences. Radiology. 1994;191(2):413–9.
10. Peterfy CG, Vandijke CF, Lu Y, Nguyen A, Connick TJ, Kneeland JB, et al. Quantification of the volume of articular-cartilage in the metacarpophalangeal joints of the hand – accuracy and precision of 3-dimensional Mr-imaging. Am J Roentgenol. 1995;165(2):371–5.
11. Disler DG, McCauley TR, Kelman CG, Fuchs MD, Ratner LM, Wirth CR, et al. Fat-suppressed three-dimensional spoiled gradient-echo MR imaging of hyaline cartilage defects in the knee: comparison with standard MR imaging and arthroscopy. Am J Roentgenol. 1996;167(1):127–32.
12. Potter HG, Linklater JM, Allen AA, Hannafin JA, Haas SB. Magnetic resonance imaging of articular cartilage in the knee – an evaluation with use of fast-spin-echo imaging. J Bone Joint Surg Am. 1998;80A(9):1276–84.
13. Kawahara Y, Uetani M, Nakahara N, Doiguchi Y, Nishiguchi M, Futagawa S, et al. Fast spin-echo MR of the articular cartilage in the osteoarthrotic knee – correlation of MR and arthroscopic findings. Acta Radiol. 1998;39(2):120–5.
14. Trattnig S, Huber M, Breitenseher MJ, Trnka HJ, Rand T, Kaider A, et al. Imaging articular cartilage defects with 3D fat-suppressed echo planar imaging: comparison with conventional 3D fat-suppressed gradient echo sequence and correlation with histology. J Comput Assist Tomogr. 1998;22(1):8–14.
15. Recht M, Bobic V, Burstein D, Disler D, Gold G, Gray M, et al. Magnetic resonance imaging of articular cartilage. Clin Orthop Relat Res. 2001;391:S379–S96.
16. Recht MP, Piraino DW, Paletta GA, Schils JP, Belhobek GH. Accuracy of fat-suppressed three-dimensional spoiled gradient-echo FLASH MR imaging in the detection of patellofemoral articular cartilage abnormalities. Radiology. 1996;198(1):209–12.
17. Roemer FW, Kwoh CK, Hannon MJ, Crema MD, Moore CE, Jakicic JM, et al. Semiquantitative assessment of focal cartilage damage at 3T MRI: a comparative study of dual echo at steady state (DESS) and intermediate-weighted (IW) fat suppressed fast spin echo sequences. Eur J Radiol. 2011;80(2):e126–31.
18. Mohr A. The value of water-excitation 3D FLASH and fat-saturated PDw TSE MR imaging for detecting and grading articular cartilage lesions of the knee. Skeletal Radiol. 2003;32(7):396–402.
19. Rubenstein JD, Li JG, Majumdar S, Henkelman RM. Image resolution and signal-to-noise ratio requirements for MR imaging of degenerative cartilage. AJR Am J Roentgenol. 1997;169(4):1089–96.
20. Notohamiprodjo M, Horng A, Pietschmann MF, Muller PE, Horger W, Park J, et al. MRI of the knee at 3T: first clinical results with an isotropic PDfs-weighted 3D-TSE-sequence. Invest Radiol. 2009;44(9):585–97.
21. Constable RT, Anderson AW, Zhong J, Gore JC. Factors influencing contrast in fast spin-Echo Mr imaging. Magn Reson Imaging. 1992;10(4):497–511.

22. Yao L, Gentili A, Thomas A. Incidental magnetization transfer contrast in fast spin-echo imaging of cartilage. J Magn Reson Imaging. 1996;6(1):180–4.
23. Bredella MA, Tirman PFJ, Peterfy CG, Zarlingo M, Feller JF, Bost FW, et al. Accuracy of T2-weighted fast spin-echo MR imaging with fat saturation in detecting cartilage defects in the knee: comparison with arthroscopy in 130 patients. Am J Roentgenol. 1999;172(4):1073–80.
24. Lichy MP, Wietek BM, Mugler JP 3rd, Horger W, Menzel MI, Anastasiadis A, et al. Magnetic resonance imaging of the body trunk using a single-slab, 3-dimensional, T2-weighted turbo-spin-echo sequence with high sampling efficiency (SPACE) for high spatial resolution imaging: initial clinical experiences. Invest Radiol. 2005;40(12):754–60.
25. Hardy PA, Recht MP, Piraino D, Thomasson D. Optimization of a dual echo in the steady state (DESS) free-precession sequence for imaging cartilage. J Magn Reson Imaging. 1996;6(2):329–35.
26. Domayer SE, Kutscha-Lissberg F, Welsch G, Dorotka R, Nehrer S, Gabler C, et al. T2 mapping in the knee after microfracture at 3.0 T: correlation of global T2 values and clinical outcome - preliminary results. Osteoarthritis Cartilage. 2008;16(8):903–8.
27. Welsch GH, Mamisch TC, Domayer SE, Dorotka R, Kutscha-Lissberg F, Marlovits S, et al. Cartilage T2 assessment at 3-T MR imaging: in vivo differentiation of normal hyaline cartilage from reparative tissue after two cartilage repair procedures – initial experience. Radiology. 2008;247(1):154–61.
28. Eckstein F, Hudelmaier M, Wirth W, Kiefer B, Jackson R, Yu J, et al. Double echo steady state magnetic resonance imaging of knee articular cartilage at 3 tesla: a pilot study for the osteoarthritis initiative. Ann Rheum Dis. 2006;65(4):433–41.
29. Moriya S, Miki Y, Kanagaki M, Matsuno Y, Miyati T. 90 degrees -flip-angle three-dimensional double-echo steady-state (3D-DESS) magnetic resonance imaging of the knee: isovoxel cartilage imaging at 3T. Eur J Radiol. 2014;83(8):1429–32.
30. Weckbach S, Mendlik T, Horger W, Wagner S, Reiser MF, Glaser C. Quantitative assessment of patellar cartilage volume and thickness at 3.0 tesla comparing a 3D-fast low angle shot versus a 3D-true fast imaging with steady-state precession sequence for reproducibility. Invest Radiol. 2006;41(2):189–97.
31. Duc SR, Pfirrmann CWA, Koch PP, Zanetti M, Hodler J. Internal knee derangement assessed with 3-minute three-dimensional isovoxel true FISP MR sequence: preliminary study. Radiology. 2008;246(2):526–35.
32. Kornaat PR, Reeder SB, Koo S, Brittain JH, Yu H, Andriacchi TP, et al. MR imaging of articular cartilage at 1.5T and 3.0T: comparison of SPGR and SSFP sequences. Osteoarthritis Cartilage. 2005;13(4):338–44.
33. Duc SR, Koch P, Schmid MR, Horger W, Hodler J, Pfirrmann CWA. Diagnosis of articular cartilage abnormalities of the knee: prospective clinical evaluation of a 3D water-excitation true FISP sequence. Radiology. 2007;243(2):475–82.
34. Eckstein F, Wirth W. Quantitative cartilage imaging in knee osteoarthritis. Arthritis. 2011;2011:475684.
35. Eckstein F, Boudreau RM, Wang Z, Hannon MJ, Wirth W, Cotofana S, et al. Trajectory of cartilage loss within 4 years of knee replacement--a nested case-control study from the osteoarthritis initiative. Osteoarthritis Cartilage. 2014;22(10):1542–9.
36. Hunter DJ, Lo GH, Gale D, Grainger AJ, Guermazi A, Conaghan PG. The reliability of a new scoring system for knee osteoarthritis MRI and the validity of bone marrow lesion assessment: BLOKS (Boston Leeds osteoarthritis knee score). Ann Rheum Dis. 2008;67(2):206–11.
37. Pang J, Driban JB, Destenaves G, Miller E, Lo GH, Ward RJ, et al. Quantification of bone marrow lesion volume and volume change using semi-automated segmentation: data from the osteoarthritis initiative. BMC Musculoskelet Disord. 2013;14:3.
38. Pelletier JP, Roubille C, Raynauld JP, Abram F, Dorais M, Delorme P, et al. Disease-modifying effect of strontium ranelate in a subset of patients from the phase III knee osteoarthritis study SEKOIA using quantitative MRI: reduction in bone marrow lesions protects against cartilage loss. Ann Rheum Dis. 2015;74(2):422–9.
39. Eckstein F, Yang M, Guermazi A, Roemer FW, Hudelmaier M, Picha K, et al. Reference values and Z-scores for subregional femorotibial cartilage thickness–results from a large population-based sample (Framingham) and comparison with the non-exposed osteoarthritis initiative reference cohort. Osteoarthritis Cartilage. 2010;18(10):1275–83.
40. Sommer FG, Jeffrey RB Jr, Rubin GD, Napel S, Rimmer SA, Benford J, et al. Detection of ureteral calculi in patients with suspected renal colic: value of reformatted noncontrast helical CT. AJR Am J Roentgenol. 1995;165(3):509–13. Epub 1995/09/01.
41. Peterfy CG, Guermazi A, Zaim S, Tirman PF, Miaux Y, White D, et al. Whole-Organ Magnetic Resonance Imaging Score (WORMS) of the knee in osteoarthritis. Osteoarthritis Cartilage. 2004;12(3):177–90.
42. Horng A, Raya JG, Stockinger M, Notohamiprodjo M, Pietschmann M, Hoehne-Hueckstaedt U, et al. Topographic deformation patterns of knee cartilage after exercises with high knee flexion: an in vivo 3D MRI study using voxel-based analysis at 3T. Eur Radiol. 2015;25(6):1731–41.
43. Frobell RB, Nevitt MC, Hudelmaier M, Wirth W, Wyman BT, Benichou O, et al. Femorotibial subchondral bone area and regional cartilage thickness: a cross-sectional description in healthy reference cases and various radiographic stages of osteoarthritis in 1,003 knees from the osteoarthritis initiative. Arthritis Care Res (Hoboken). 2010;62(11):1612–23.
44. Eckstein F, Cicuttini F, Raynauld JP, Waterton JC, Peterfy C. Magnetic resonance imaging (MRI) of articular cartilage in knee osteoarthritis (OA): mor-

phological assessment. Osteoarthritis Cartilage. 2006;14(Suppl A):A46–75.
45. Micheel CM, Ball JR, editors. Evaluation of biomarkers and surrogate endpoints in chronic disease. Washington, DC: National Academies Press; 2010.
46. Rubenstein JD, Li JG, Majumdar S, Henkelman RM. Image resolution and signal-to-noise ratio requirements for MR imaging of degenerative cartilage. Am J Roentgenol. 1997;169(4):1089–96.
47. Gagliardi JA, Chung EM, Chandnani VP, Kesling KL, Christensen KP, Null RN, et al. Detection and staging of chondromalacia patellae – relative efficacies of conventional Nir imaging, Mr arthrography, and Ct arthrography. Am J Roentgenol. 1994;163(3):629–36.
48. Juras V, Welsch G, Bar P, Kronnerwetter C, Fujita H, Trattnig S. Comparison of 3T and 7T MRI clinical sequences for ankle imaging. Eur J Radiol. 2012;81(8):1846–50.
49. Rubin GD, Napel S. Increased scan pitch for vascular and thoracic spiral CT. Radiology. 1995;197(1):316–7. Epub 1995/10/01.
50. Springer E, Bohndorf K, Juras V, Szomolanyi P, Zbyn S, Schreiner MM, Schmitt B and Trattnig S. Comparison of Routine Knee Magnetic Resonance Imaging at 3 T and 7 T. Invest Radiol. 2017;52:42–54.
51. Welsch GH, Juras V, Szomolanyi P, Mamisch TC, Baer P, Kronnerwetter C, et al. Magnetic resonance imaging of the knee at 3 and 7 tesla: a comparison using dedicated multi-channel coils and optimised 2D and 3D protocols. Eur Radiol. 2012;22(9):1852–9.
52. Alparslan L, Winalski CS, Boutin RD, Minas T. Postoperative magnetic resonance imaging of articular cartilage repair. Semin Musculoskelet Radiol. 2001;5(4):345–63.
53. Choi YS, Potter HG, Chun TJMR. Imaging of cartilage repair in the knee and ankle. Radiographics. 2008;28(4):1043–59.
54. Guermazi A, Roemer FW, Alizai H, Winalski CS, Welsch G, Brittberg M, et al. State of the art: MR imaging after knee cartilage repair surgery. Radiology. 2015;277(1):23–43.
55. Farr J, Cole B, Dhawan A, Kercher J, Sherman S. Clinical cartilage restoration: evolution and overview. Clin Orthop Relat Res. 2011;469(10):2696–705.
56. Link TM, Mischung J, Wortler K, Burkart A, Rummeny EJ, Imhoff AB. Normal and pathological MR findings in osteochondral autografts with longitudinal follow-up. Eur Radiol. 2006;16(1):88–96.
57. Sanders TG, Mentzer KD, Miller MD, Morrison WB, Campbell SE, Penrod BJ. Autogenous osteochondral "plug" transfer for the treatment of focal chondral defects: postoperative MR appearance with clinical correlation. Skelet Radiol. 2001;30(10):570–8.
58. Herber S, Runkel M, Pitton MB, Kalden P, Thelen M, Kreitner KF. Indirect MR-arthrography in the follow up of autologous osteochondral transplantation. Rofo. 2003;175(2):226–33. Indirekte MR-Arthrographie zur Verlaufskontrolle nach autologer osteochondraler Transplantation.
59. Trattnig S, Ba-Ssalamah A, Pinker K, Plank C, Vecsei V, Marlovits S. Matrix-based autologous chondrocyte implantation for cartilage repair: noninvasive monitoring by high-resolution magnetic resonance imaging. Magn Reson Imaging. 2005;23(7):779–87. Epub 2005/10/11.
60. Trattnig S, Pinker K, Krestan C, Plank C, Millington S, Marlovits S. Matrix-based autologous chondrocyte implantation for cartilage repair with HyalograftC: two-year follow-up by magnetic resonance imaging. Eur J Radiol. 2006;57(1):9–15. Epub 2005/09/27.
61. Trattnig S, Millington SA, Szomolanyi P, Marlovits S. MR imaging of osteochondral grafts and autologous chondrocyte implantation. Eur Radiol. 2007;17(1):103–18. Epub 2006/06/28.
62. Marlovits S, Striessnig G, Resinger CT, Aldrian SM, Vecsei V, Imhof H, et al. Definition of pertinent parameters for the evaluation of articular cartilage repair tissue with high-resolution magnetic resonance imaging. Eur J Radiol. 2004;52(3):310–9. Epub 2004/11/17.
63. Trattnig S, Ohel K, Mlynarik V, Juras V, Zbyn S, Korner A. Morphological and compositional monitoring of a new cell-free cartilage repair hydrogel technology – GelrinC by MR using semi-quantitative MOCART scoring and quantitative T2 index and new zonal T2 index calculation. Osteoarthritis Cartilage. 2015;23(12):2224–32.
64. Welsch GH, Zak L, Mamisch TC, Resinger C, Marlovits S, Trattnig S. Three-dimensional magnetic resonance observation of cartilage repair tissue (MOCART) score assessed with an isotropic three-dimensional true fast imaging with steady-state precession sequence at 3.0 tesla. Invest Radiol. 2009;44(9):603–12. Epub 2009/08/21.
65. Welsch GH, Zak L, Mamisch TC, Paul D, Lauer L, Mauerer A, et al. Advanced morphological 3D magnetic resonance observation of cartilage repair tissue (MOCART) scoring using a new isotropic 3D proton-density, turbo spin echo sequence with variable flip angle distribution (PD-SPACE) compared to an isotropic 3D steady-state free precession sequence (true-FISP) and standard 2D sequences. J Magn Reson Imaging. 2011;33(1):180–8. Epub 2010/12/25.
66. Roemer FW, Guermazi A, Trattnig S, Apprich S, Marlovits S, Niu J, et al. Whole joint MRI assessment of surgical cartilage repair of the knee: cartilage repair osteoarthritis knee score (CROAKS). Osteoarthritis Cartilage. 2014;22(6):779–99.
67. Hunter DJ, Guermazi A, Lo GH, Grainger AJ, Conaghan PG, Boudreau RM, et al. Evolution of semi-quantitative whole joint assessment of knee OA: MOAKS (MRI osteoarthritis knee score). Osteoarthritis Cartilage. 2011;19(8):990–1002.
68. Buckwalter JA, Mankin HJ. Articular cartilage: degeneration and osteoarthritis, repair, regeneration, and transplantation. Instr Course Lect. 1998;47:487–504.

69. Poole AR, Kojima T, Yasuda T, Mwale F, Kobayashi M, Laverty S. Composition and structure of articular cartilage – a template for tissue repair. Clin Orthop Relat Res. 2001;391:S26–33.
70. Maroudas A. Physicochemical properties of cartilage in the light of ion exchange theory. Biophys J. 1968;8(5):575–95.
71. Maroudas A, Muir H, Wingham J. The correlation of fixed negative charge with glycosaminoglycan content of human articular cartilage. Biochim Biophys Acta. 1969;177(3):492–500.
72. Grodzinsky AJ. Electromechanical and physicochemical properties of connective tissue. Crit Rev Biomed Eng. 1983;9(2):133–99.
73. Goodwin DW, Zhu HQ, Dunn JF. In vitro MR imaging of hyaline cartilage: correlation with scanning electron microscopy. Am J Roentgenol. 2000;174(2):405–9.
74. Bachmann G, Basad E, Lommel D, Steinmeyer J. MRI in the follow-up after MACI((R)) or microfracture. Radiologe. 2004;44(8):773–82.
75. Bentley G, Biant LC, Carrington RWJ, Akmal M, Goldberg A, Williams AM, et al. A prospective, randomised comparison of autologous chondrocyte implantation versus mosaicplasty for osteochondral defects in the knee. J Bone Joint Surg. 2003;85B(2):223–30.
76. Brittberg M, Lindahl A, Nilsson A, Ohlsson C, Isaksson O, Peterson L. Treatment of deep cartilage defects in the knee with autologous chondrocyte transplantation. N Engl J Med. 1994;331(14):889–95.
77. Gudas R, Kalesinskas RJ, Kimtys V, Stankevicius E, Toliusis V, Bernotavicius G, et al. A prospective randomized clinical study of mosaic osteochondral autologous transplantation versus microfracture for the treatment of osteochondral defects in the knee joint in young athletes. Arthroscopy. 2005;21(9):1066–75.
78. Gudas R, Stankevicius E, Monastyreckiene E, Pranys D, Kalesinskas RJ. Osteochondral autologous transplantation versus microfracture for the treatment of articular cartilage defects in the knee joint in athletes. Knee surgery sports traumatology. Arthroscopy. 2006;14(9):834–42.
79. Knutsen G, Drogset JO, Engebretsen L, Grontvedt T, Isaksen V, Ludvigsen TC, et al. A randomized trial comparing autologous chondrocyte implantation with microfracture. J Bone Joint Surg Am. 2007;89A(10):2105–12.
80. Knutsen G, Engebretsen L, Ludvigsen TC, Drogset JO, Grontvedt T, Solheim E, et al. Autologous chondrocyte implantation compared with microfracture in the knee – a randomized trial. J Bone Joint Surg Am. 2004;86A(3):455–64.
81. Nieminen MT, Nissi MJ, Mattila L, Kiviranta I. Evaluation of chondral repair using quantitative MRI. J Magn Reson Imaging. 2012;36(6):1287–99.
82. Burstein D, Velyvis J, Scott KT, Stock KW, Kim YJ, Jaramillo D, et al. Protocol issues for delayed Gd(DTPA)(2-)-enhanced MRI: (dGEMRIC) for clinical evaluation of articular cartilage. Magn Reson Med. 2001;45(1):36–41.
83. Bashir A, Gray ML, Burstein D. Gd-DTPA(2-) as a measure of cartilage degradation. Magn Reson Med. 1996;36(5):665–73.
84. Borthakur A, Shapiro EM, Beers J, Kudchodkar S, Kneeland JB, Reddy R. Sensitivity of MRI to proteoglycan depletion in cartilage: comparison of sodium and proton MRI. Osteoarthritis Cartilage. 2000;8(4):288–93.
85. Ling W, Regatte RR, Navon G, Jerschow A. Assessment of glycosaminoglycan concentration in vivo by chemical exchange-dependent saturation transfer (gagCEST). Proc Natl Acad Sci U S A. 2008;105(7):2266–70. Epub 2008/02/13.
86. Windschuh J, Zaiss M, Ehses P, Lee JS, Jerschow A, et al. Assessment of frequency drift on CEST MRI and dynamic correction: application to gagCEST at 7 T. Magn Reson Med. 2019;81(1):573–82.
87. Trattnig S, Raudner M, Schreiner M, Roemer F, Bohndorf K. Biochemical cartilage imaging-update 2019. Radiologe. 2019;59(8):742–49.
88. Mosher TJ, Dardzinski BJ. Cartilage MRI T2 relaxation time mapping: overview and applications. Semin Musculoskelet Radiol. 2004;8(4):355–68.
89. Nebelung S, Post M, Knobe M, Tingart M, Emans P, et al. Detection of early-stage degeneration in human articular cartilage by multiparametric MR imaging mapping of tissue functionality. Sci Rep. 2019;9(1):5895.
90. Welsch GH, Mamisch TC, Hughes T, Zilkens C, Quirbach S, Scheffler K, et al. In vivo biochemical 7.0 tesla magnetic resonance – preliminary results of dGEMRIC, zonal T2, and T2 * mapping of articular cartilage. Invest Radiol. 2008;43(9):619–26.
91. Williams A, Qian Y, Bear D, Chu CR. Assessing degeneration of human articular cartilage with ultrashort echo time (UTE) T2* mapping. Osteoarthritis Cartilage. 2010;18(4):539–46.
92. Pauli C, Bae WC, Lee M, Lotz M, Bydder GM, D'Lima DL, et al. Ultrashort-echo time MR imaging of the patella with bicomponent analysis: correlation with histopathologic and polarized light microscopic findings. Radiology. 2012;264(2):484–93.
93. Mamisch TC, Hughes T, Mosher TJ, Mueller C, Trattnig S, Boesch C, et al. T2 star relaxation times for assessment of articular cartilage at 3 T: a feasibility study. Skelet Radiol. 2012;41(3):287–92.
94. Bittersohl B, Hosalkar HS, Miese FR, Schibensky J, Konig DP, Herten M, et al. Zonal T2* and T1Gd assessment of knee joint cartilage in various histological grades of cartilage degeneration: an observational in vitro study. BMJ Open. 2015;5(2):e006895.
95. Juras V, Mlynarik V, Szomolanyi P, Valkovič L, Trattnig S. Magnetic resonance imaging of the musculoskeletal system at 7T: morphological imaging and beyond. Top Magn Reson Imaging. 2019;28(3):125–35.
96. Regatte RR, Akella SVS, Lonner JH, Kneeland JB, Reddy R. T-1p relaxation mapping in human osteo-

arthritis (OA) cartilage: comparison of T-1p with T-2. J Magn Reson Imaging. 2006;23(4):547–53.
97. Mlynarik V, Szomolanyi P, Toffanin R, Vittur F, Trattnig S. Transverse relaxation mechanisms in articular cartilage. J Magn Reson. 2004;169(2):300–7. Epub 2004/07/21.
98. Goodwin DW, Wadghiri YZ, Dunn JF. Micro-imaging of articular cartilage: T2, proton density, and the magic angle effect. Acad Radiol. 1998;5(11):790–8.
99. Smith HE, Mosher TJ, Dardzinski BJ, Collins BG, Collins CM, Yang QX, et al. Spatial variation in cartilage T2 of the knee. J Magn Reson Imaging. 2001;14(1):50–5.
100. Watrin-Pinzano A, Ruaud JP, Cheli Y, Gonord P, Grossin L, Bettembourg-Brault I, et al. Evaluation of cartilage repair tissue after biomaterial implantation in rat patella by using T2 mapping. Magn Reson Mater Phys Biol Med. 2004;17(3–6):219–28.
101. White LM, Sussman MS, Hurtig M, Probyn L, Tomlinson G, Kandel R. Cartilage T2 assessment: differentiation of normal hyaline cartilage and reparative tissue after arthroscopic cartilage repair in equine subjects. Radiology. 2006;241(2):407–14.
102. Domayer SE, Apprich S, Stelzeneder D, Hirschfeld C, Sokolowski M, Kronnerwetter C, et al. Cartilage repair of the ankle: first results of T2 mapping at 7.0 T after microfracture and matrix associated autologous cartilage transplantation. Osteoarthritis Cartilage. 2012;20(8):829–36.
103. Welsch GH, Apprich S, Zbyn S, Mamisch TC, Mlynarik V, Scheffler K, et al. Biochemical (T2, T2* and magnetisation transfer ratio) MRI of knee cartilage: feasibility at ultra-high field (7T) compared with high field (3T) strength. Eur Radiol. 2011;21(6):1136–43.
104. Juras V, Zbyn S, Mlynarik V, Szomolanyi P, Hager B, Baer P, et al. The compositional difference between ankle and knee cartilage demonstrated by T2 mapping at 7 tesla MR. Eur J Radiol. 2016;85(4):771–7.
105. Martín Noguerol T, Raya JG, Wessell DE, Vilanova JC, Rossi I, et al. Functional MRI for evaluation of hyaline cartilage extracelullar matrix, a physiopathological-based approach. Br J Radiol. 2019;92(1103):20190443. https://doi.org/10.1259/bjr.20190443.
106. Li Z, Wang H, Lu Y, Jiang M, Chen Z, et al. Diagnostic value of T1ρ and T2 mapping sequences of 3D fat-suppressed spoiled gradient (FS SPGR-3D) 3.0-T magnetic resonance imaging for osteoarthritis. Medicine (Baltimore). 2019;98(1):e13834.
107. Colotti R, Omoumi P, Bonanno G, Ledoux JB, van Heeswijk RB. Isotropic three-dimensional T2 mapping of knee cartilage: Development and validation. J Magn Reson Imaging. 2018;47(2):362–71.
108. Joseph GB, Nevitt MC, McCulloch CE, Neumann J, Lynch JA, et al. Associations between molecular biomarkers and MR-based cartilage composition and knee joint morphology: data from the Osteoarthritis Initiative. Osteoarthritis Cartilage. 2018;26(8):1070–77.
109. Liebl H, Joseph G, Nevitt MC, Singh N, Heilmeier U, Subburaj K, et al. Early T2 changes predict onset of radiographic knee osteoarthritis: data from the osteoarthritis initiative. Ann Rheum Dis. 2015;74(7):1353–9.
110. Apprich S, Mamisch TC, Welsch GH, Stelzeneder D, Albers C, Totzke U, et al. Quantitative T2 mapping of the patella at 3.0T is sensitive to early cartilage degeneration, but also to loading of the knee. Eur J Radiol. 2012;81(4):e438–43.
111. Su F, Pedoia V, Teng HL, Kretzschmar M, Lau BC, McCulloch CE, et al. The association between MR T1rho and T2 of cartilage and patient-reported outcomes after ACL injury and reconstruction. Osteoarthritis Cartilage. 2016;24(7):1180–9.
112. Munukka M, Waller B, Rantalainen T, Hakkinen A, Nieminen MT, Lammentausta E, et al. Efficacy of progressive aquatic resistance training for tibiofemoral cartilage in postmenopausal women with mild knee osteoarthritis: a randomised controlled trial. Osteoarthritis Cartilage. 2016;24(10):1708–17.
113. Trattnig S, Mamisch TC, Welsch GH, Glaser C, Szomolanyi P, Gebetsroither S, et al. Quantitative T-2 mapping of matrix-associated autologous chondrocyte transplantcation at 3 tesla – an in vivo cross-sectional study. Invest Radiol. 2007;42(6):442–8.
114. Liney GP, Knowles AJ, Manton DJ, Turnbull LW, Blackband SJ, Horsman A. Comparison of conventional single echo and multi-echo sequences with a fast spin-echo sequence for quantitative T2 mapping: application to the prostate. J Magn Reson Imaging. 1996;6(4):603–7.
115. Heule R, Ganter C, Bieri O. Triple echo steady-state (TESS) relaxometry. Magn Reson Med. 2014;71(1):230–7.
116. Juras V, Bohndorf K, Heule R, Kronnerwetter C, Szomolanyi P, Hager B, Bieri O, Zbyn S and Trattnig S. A comparison of multi-echo spin-echo and triple-echo steady-state T2 mapping for in vivo evaluation of articular cartilage. Eur Radiol. 2016;26:1905–12.
117. Schoenbauer E, Szomolanyi P, Shiomi T, Juras V, Zbyn S, Zak L, et al. Cartilage evaluation with biochemical MR imaging using in vivo knee compression at 3T-comparison of patients after cartilage repair with healthy volunteers. J Biomech. 2015;48(12):3349–55.
118. Du J, Takahashi AM, Chung CB. Ultrashort TE spectroscopic imaging (UTESI): application to the imaging of short T2 relaxation tissues in the musculoskeletal system. J Magn Reson Imaging. 2009;29(2):412–21.
119. Chavhan GB, Babyn PS, Thomas B, Shroff MM, Haacke EM. Principles, techniques, and applications of T2*-based MR imaging and its special applications. Radiographics. 2009;29(5):1433–49.
120. Maier CF, Tan SG, Hariharan H, Potter HG. T2 quantitation of articular cartilage at 1.5 T. J Magn Reson Imaging. 2003;17(3):358–64.

121. Lusse S, Claassen H, Gehrke T, Hassenpflug J, Schunke M, Heller M, et al. Evaluation of water content by spatially resolved transverse relaxation times of human articular cartilage. Magn Reson Imaging. 2000;18(4):423–30.
122. Bittersohl B, Miese FR, Hosalkar HS, Mamisch TC, Antoch G, Krauspe R, et al. T2* mapping of acetabular and femoral hip joint cartilage at 3 T: a prospective controlled study. Invest Radiol. 2012;47(7):392–7.
123. Robson MD, Gatehouse PD, Bydder M, Bydder GM. Magnetic resonance: an introduction to ultrashort TE (UTE) imaging. J Comput Assist Tomogr. 2003;27(6):825–46.
124. Bittersohl B, Miese FR, Hosalkar HS, Herten M, Antoch G, Krauspe R, et al. T2* mapping of hip joint cartilage in various histological grades of degeneration. Osteoarthritis Cartilage. 2012;20(7):653–60.
125. Welsch GH, Trattnig S, Hughes T, Quirbach S, Olk A, Blanke M, et al. T2 and T2* mapping in patients after matrix-associated autologous chondrocyte transplantation: initial results on clinical use with 3.0-tesla MRI. Eur Radiol. 2010;20(6):1515–23.
126. Regatte RR, Akella SVS, Wheaton AJ, Borthakur A, Kneeland JB, Reddy R. T-1 rho-relaxation mapping of human femoral-tibial cartilage in vivo. J Magn Reson Imaging. 2003;18(3):336–41.
127. Menezes NM, Gray ML, Hartke JR, Burstein D. T-2 and T-1, MRI in articular cartilage systems. Magn Reson Med. 2004;51(3):503–9.
128. van Tiel J, Kotek G, Reijman M, Bos PK, Bron EE, Klein S, et al. Is T1rho mapping an alternative to delayed gadolinium-enhanced MR imaging of cartilage in the assessment of Sulphated glycosaminoglycan content in human osteoarthritic knees? An in vivo validation study. Radiology. 2016;279(2):523–31.
129. Prasad AP, Nardo L, Schooler J, Joseph GB, Link TM. T(1)rho and T(2) relaxation times predict progression of knee osteoarthritis. Osteoarthritis Cartilage. 2013;21(1):69–76.
130. Holtzman DJ, Theologis AA, Carballido-Gamio J, Majumdar S, Li X, Benjamin C. T(1rho) and T(2) quantitative magnetic resonance imaging analysis of cartilage regeneration following microfracture and mosaicplasty cartilage resurfacing procedures. J Magn Reson Imaging. 2010;32(4):914–23.
131. Theologis AA, Schairer WW, Carballido-Gamio J, Majumdar S, Li X, Ma CB. Longitudinal analysis of T1rho and T2 quantitative MRI of knee cartilage laminar organization following microfracture surgery. Knee. 2012;19(5):652–7.
132. Wolff SD, Chesnick S, Frank JA, Lim KO, Balaban RS. Magnetization transfer contrast – Mr-imaging of the knee. Radiology. 1991;179(3):623–8.
133. Gray ML, Burstein D, Lesperance LM, Gehrke L. Magnetization-transfer in cartilage and its constituent macromolecules. Magn Reson Med. 1995;34(3):319–25.
134. Kim DK, Ceckler TL, Hascall VC, Calabro A, Balaban RS. Analysis of water-macromolecule proton magnetization transfer in articular-cartilage. Magn Reson Med. 1993;29(2):211–5.
135. Seo GS, Aoki J, Moriya H, Karakida O, Sone S, Hidaka H, et al. Hyaline cartilage: in vivo and in vitro assessment with magnetization transfer imaging. Radiology. 1996;201(2):525–30.
136. Wolff SD, Balaban RS. Magnetization transfer contrast (Mtc) and tissue water proton relaxation Invivo. Magn Reson Med. 1989;10(1):135–44.
137. Wolff SD, Eng J, Balaban RS. Magnetization transfer contrast – method for improving contrast in gradient-recalled-Echo images. Radiology. 1991;179(1):133–7.
138. Palmieri F, De Keyzer F, Maes F, Van Breuseghem I. Magnetization transfer analysis of cartilage repair tissue: a preliminary study. Skelet Radiol. 2006;35(12):903–8.
139. Bieri O, Scheffler K. Optimized balanced steady-state free precession magnetization transfer imaging. Magn Reson Med. 2007;58(3):511–8.
140. Welsch GH, Trattnig S, Scheffler K, Szomonanyi P, Quirbach S, Marlovits S, et al. Magnetization transfer contrast and T2 mapping in the evaluation of cartilage repair tissue with 3T MRI. J Magn Reson Imaging. 2008;28(4):979–86.
141. Potter K, Butler JJ, Horton WE, Spencer RGS. Response of engineered cartilage tissue to biochemical agents as studied by proton magnetic resonance microscopy. Arthritis Rheum. 2000;43(7):1580–90.
142. Vahlensieck M, Dombrowski F, Leutner C, Wagner U, Reiser M. Magnetization-Transfer Contrast (Mtc) and Mtc-subtraction – enhancement of cartilage lesions and Intracartilaginous degeneration in-vitro. Skelet Radiol. 1994;23(7):535–9.
143. Kogan F, Hariharan H, Reddy R. Chemical Exchange Saturation Transfer (CEST) imaging: description of technique and potential clinical applications. Curr Radiol Rep. 2013;1(2):102–14. Epub 2013/06/05.
144. Schmitt B, Zbyn S, Stelzeneder D, Jellus V, Paul D, Lauer L, et al. Cartilage quality assessment by using glycosaminoglycan chemical exchange saturation transfer and (23)Na MR imaging at 7 T. Radiology. 2011;260(1):257–64.
145. Krusche-Mandl I, Schmitt B, Zak L, Apprich S, Aldrian S, Juras V, et al. Long-term results 8 years after autologous osteochondral transplantation: 7 T gagCEST and sodium magnetic resonance imaging with morphological and clinical correlation. Osteoarthritis Cartilage. 2012;20(5):357–63.
146. Schreiner MM, Zbyn S, Schmitt B, Weber M, Domayer S, Windhager R, et al. Reproducibility and regional variations of an improved gagCEST protocol for the in vivo evaluation of knee cartilage at 7 T. MAGMA. 2016;29(3):513–21.
147. Singh A, Haris M, Cai K, Kassey VB, Kogan F, Reddy D, et al. Chemical exchange saturation transfer magnetic resonance imaging of human knee cartilage at 3 T and 7 T. Magn Reson Med. 2012;68(2):588–94. Epub 2012/01/04.

148. Zaiss M, Bachert P. Chemical exchange saturation transfer (CEST) and MR Z-spectroscopy in vivo: a review of theoretical approaches and methods. Phys Med Biol. 2013;58(22):R221–69. Epub 2013/11/10.
149. Kim M, Gillen J, Landman BA, Zhou J, van Zijl PC. Water saturation shift referencing (WASSR) for chemical exchange saturation transfer (CEST) experiments. Magn Reson Med. 2009;61(6):1441–50. Epub 2009/04/10.
150. Krishnamoorthy G, Nanga RPR, Bagga P, Hariharan H and Reddy R. High quality three-dimensional gagCEST imaging of in vivo human knee cartilage at 7 Tesla. Magn Reson Med. 2017;77:1866–73.
151. Burstein D, Bashir A, Gray ML. MRI techniques in early stages of cartilage disease. Invest Radiol. 2000;35(10):622–38.
152. Watanabe A, Wada Y, Obata T, Ueda T, Tamura M, Ikehira H, et al. Delayed gadolinium-enhanced MR to determine glycosaminoglycan concentration in reparative cartilage after autologous chondrocyte implantation: preliminary results. Radiology. 2006;239(1):201–8.
153. Bashir A, Gray ML, Boutin RD, Burstein D. Glycosaminoglycan in articular cartilage: in vivo assessment with delayed Gd(DTPA)(2-)-enhanced MR imaging. Radiology. 1997;205(2):551–8.
154. Tiderius CJ, Olsson LE, Leander P, Ekberg O, Dahlberg L. Delayed gadolinium-enhanced MRI of cartilage (dGEMRIC) in early knee osteoarthritis. Magn Reson Med. 2003;49(3):488–92.
155. Williams A, Gillis A, McKenzie C, Po B, Sharma L, Micheli L, et al. Glycosaminoglycan distribution in cartilage as determined by delayed gadolinium-enhanced MRI of cartilage (dGEMRIC): potential clinical applications. Am J Roentgenol. 2004;182(1):167–72.
156. Rubin GD, Napel S. Helical CT angiography of renal artery stenosis. AJR Am J Roentgenol. 1997;168(4):1109–11. Epub 1997/04/01.
157. Trattnig S, Marlovits S, Gebetsroither S, Szomolanyi P, Welsch GH, Salomonowitz E, et al. Three-dimensional delayed gadolinium-enhanced MRI of cartilage (dGEMRIC) for in vivo evaluation of reparative cartilage after matrix-associated autologous chondrocyte transplantation at 3.0T: preliminary results. J Magn Reson Imaging. 2007;26(4):974–82.
158. Trattnig S, Mamisch TC, Pinker K, Domayer S, Szomolanyi P, Marlovits S, et al. Differentiating normal hyaline cartilage from post-surgical repair tissue using fast gradient echo imaging in delayed gadolinium-enhanced MRI (dGEMRIC) at 3 tesla. Eur Radiol. 2008;18(6):1251–9.
159. Kim YJ, Jaramillo D, Millis MB, Gray ML, Burstein D. Assessment of early osteoarthritis in hip dysplasia with delayed gadolinium-enhanced magnetic resonance imaging of cartilage. J Bone Joint Surg Am. 2003;85A(10):1987–92.
160. Lattanzi R, Petchprapa C, Ascani D, Babb JS, Chu D, Davidovitch RI, et al. Detection of cartilage damage in femoroacetabular impingement with standardized dGEMRIC at 3 T. Osteoarthritis Cartilage. 2014;22(3):447–56.
161. Owman H, Ericsson YB, Englund M, Tiderius CJ, Tjornstrand J, Roos EM, et al. Association between delayed gadolinium-enhanced MRI of cartilage (dGEMRIC) and joint space narrowing and osteophytes: a cohort study in patients with partial meniscectomy with 11 years of follow-up. Osteoarthritis Cartilage. 2014;22(10):1537–41.
162. Crema MD, Hunter DJ, Burstein D, Roemer FW, Li L, Eckstein F, et al. Association of changes in delayed gadolinium-enhanced MRI of cartilage (dGEMRIC) with changes in cartilage thickness in the medial tibiofemoral compartment of the knee: a 2 year follow-up study using 3.0 T MRI. Ann Rheum Dis. 2014;73(11):1935–41.
163. Vaga S, Raimondi MT, Caiani EG, Costa F, Giordano C, Perona F, et al. Quantitative assessment of intervertebral disc glycosaminoglycan distribution by gadolinium-enhanced MRI in orthopedic patients. Magn Reson Med. 2008;59(1):85–95.
164. Williams A, Shetty SK, Burstein D, Day CS, McKenzie C. Delayed gadolinium enhanced MRI of cartilage (dGEMRIC) of the first carpometacarpal (1CMC) joint: a feasibility study. Osteoarthritis Cartilage. 2008;16(4):530–2.
165. Pittschieler E, Szomolanyi P, Schmid-Schwap M, Weber M, Egerbacher M, Traxler H, et al. Delayed gadolinium-enhanced MRI of the fibrocartilage disc of the temporomandibular joint–a feasibility study. Magn Reson Imaging. 2014;32(10):1223–9.
166. Lesperance LM, Gray ML, Burstein D. Determination of fixed charge density in cartilage using nuclear magnetic resonance. J Orthop Res. 1992;10(1):1–13.
167. Reddy R, Insko EK, Noyszewski EA, Dandora R, Kneeland JB, Leigh JS. Sodium MRI of human articular cartilage in vivo. Magn Reson Med. 1998;39(5):697–701.
168. Shapiro EM, Borthakur A, Dandora R, Kriss A, Leigh JS, Reddy R. Sodium visibility and quantitation in intact bovine articular cartilage using high field (23)Na MRI and MRS. J Magn Reson. 2000;142(1):24–31.
169. Shapiro EM, Borthakur A, Gougoutas A, Reddy R. 23Na MRI accurately measures fixed charge density in articular cartilage. Magn Reson Med. 2002;47(2):284–91.
170. Pabst T, Sandstede J, Beer M, Kenn W, Neubauer S, Hahn D. Sodium T2* relaxation times in human heart muscle. J Magn Reson Imaging. 2002;15(2):215–8.
171. Jerecic R, Bock M, Nielles-Vallespin S, Wacker C, Bauer W, Schad LR. ECG-gated 23Na-MRI of the human heart using a 3D-radial projection technique with ultra-short echo times. MAGMA. 2004;16(6):297–302.
172. Borthakur A, Mellon E, Niyogi S, Witschey W, Kneeland JB, Reddy R. Sodium and T1rho MRI for molecular and diagnostic imaging of articular

cartilage. NMR Biomed. 2006;19(7):781–821. Epub 2006/11/01.
173. Rahmer J, Bornert P, Groen J, Bos C. Three-dimensional radial ultrashort echo-time imaging with T2 adapted sampling. Magn Reson Med. 2006;55(5):1075–82.
174. Nielles-Vallespin S, Weber MA, Bock M, Bongers A, Speier P, Combs SE, et al. 3D radial projection technique with ultrashort echo times for sodium MRI: clinical applications in human brain and skeletal muscle. Magn Reson Med. 2007;57(1):74–81.
175. Jordan CD, McWalter EJ, Monu UD, Watkins RD, Chen W, Bangerter NK, et al. Variability of CubeQuant T1rho, quantitative DESS T2, and cones sodium MRI in knee cartilage. Osteoarthritis Cartilage. 2014;22(10):1559–67.
176. Trattnig S, Zbyn S, Schmitt B, Friedrich K, Juras V, Szomolanyi P, et al. Advanced MR methods at ultra-high field (7 tesla) for clinical musculoskeletal applications. Eur Radiol. 2012;22(11):2338–46.
177. Madelin G, Regatte RR. Biomedical applications of sodium MRI in vivo. J Magn Reson Imaging. 2013;38(3):511–29.
178. Grushko G, Schneiderman R, Maroudas A. Some biochemical and biophysical parameters for the study of the pathogenesis of osteoarthritis: a comparison between the processes of ageing and degeneration in human hip cartilage. Connect Tissue Res. 1989;19(2–4):149–76.
179. Lohmander LS. Articular cartilage and osteoarthrosis. The role of molecular markers to monitor breakdown, repair and disease. J Anat. 1994;184(Pt 3):477–92.
180. Wheaton AJ, Borthakur A, Dodge GR, Kneeland JB, Schumacher HR, Reddy R. Sodium magnetic resonance imaging of proteoglycan depletion in an in vivo model of osteoarthritis. Acad Radiol. 2004;11(1):21–8.
181. Wheaton AJ, Borthakur A, Shapiro EM, Regatte RR, Akella SV, Kneeland JB, et al. Proteoglycan loss in human knee cartilage: quantitation with sodium MR imaging–feasibility study. Radiology. 2004;231(3):900–5.
182. Wang L, Wu Y, Chang G, Oesingmann N, Schweitzer ME, Jerschow A, et al. Rapid isotropic 3D-sodium MRI of the knee joint in vivo at 7T. J Magn Reson Imaging. 2009;30(3):606–14.
183. Madelin G, Babb J, Xia D, Chang G, Krasnokutsky S, Abramson SB, et al. Articular cartilage: evaluation with fluid-suppressed 7.0-T sodium MR imaging in subjects with and subjects without osteoarthritis. Radiology. 2013;268(2):481–91.
184. Newbould RD, Miller SR, Tielbeek JA, Toms LD, Rao AW, Gold GE, et al. Reproducibility of sodium MRI measures of articular cartilage of the knee in osteoarthritis. Osteoarthritis Cartilage. 2012;20(1):29–35.
185. Marik W, Nemec SF, Zbyn S, Zalaudek M, Ludvik B, Riegler G, et al. Changes in cartilage and tendon composition of patients with type I diabetes mellitus: identification by quantitative sodium magnetic resonance imaging at 7 T. Invest Radiol. 2016;51(4):266–72.
186. Trattnig S, Welsch GH, Juras V, Szomolanyi P, Mayerhoefer ME, Stelzeneder D, et al. 23Na MR imaging at 7 T after knee matrix-associated autologous chondrocyte transplantation preliminary results. Radiology. 2010;257(1):175–84.
187. Zbyn S, Stelzeneder D, Welsch GH, Negrin LL, Juras V, Mayerhoefer ME, et al. Evaluation of native hyaline cartilage and repair tissue after two cartilage repair surgery techniques with 23Na MR imaging at 7 T: initial experience. Osteoarthritis Cartilage. 2012;20(8):837–45.